Fabrication, Structure and Performances of Graphene Oxide Based Membrane for Water Filtration

Shen, Yang

Publication date:
2019

Document Version
Publisher's PDF, also known as Version of record

FABRICATION, STRUCTURE AND PERFORMANCES OF GRAPHENE OXIDE BASED MEMBRANE FOR WATER FILTRATION

BY
YANG SHEN

DISSERTATION SUBMITTED 2019

AALBORG UNIVERSITY
DENMARK

FABRICATION, STRUCTURE AND PERFORMANCES OF GRAPHENE OXIDE BASED MEMBRANE FOR WATER FILTRATION

by

Yang Shen

AALBORG UNIVERSITY
DENMARK

Dissertation submitted 2019

.

Dissertation submitted: February 2019

PhD supervisors: Prof. Yuanzheng Yue
Aalborg University

Associate Prof. Vittorio Boffa
Aalborg University

PhD committee: Associate Professor Thorbjørn Terndrup Nielsen (chair.)
Aalborg University

Associate Professor Gloria Berlier
Turin University

Senior Scientist Bhaskar Reddy Sudireddy
Technical University of Denmark

PhD Series: Faculty of Engineering and Science, Aalborg University

Department: Department of Chemistry and Bioscience

ISSN (online): 2446-1636
ISBN (online): 978-87-7210-392-1

Published by:
Aalborg University Press
Langagervej 2
DK – 9220 Aalborg Ø
Phone: +45 99407140
aauf@forlag.aau.dk
forlag.aau.dk

Printed in Denmark by Rosendahls, 2019

ENGLISH SUMMARY

Graphene oxide (GO) is a fantastic material, which is an oxidized form of graphene. With its unique two-dimension structure (single-atom-thick layer) and outstanding properties (e.g. high molecular selectivity), GO has been applied in many research fields, such as water purification membranes, sensors, semiconductors, drugs carrier and catalysis. The goal of this PhD project is to investigate the structural and chemical evolution of GO during thermal treatment and to explore the potential of reduced GO (rGO) materials in membrane applications.

The thermal reduction mechanism and kinetics of Hummers' GO were studied. During the low-temperature heat treatment, the reduction process of GO could be divided into 3 steps: Step 1, below 160 °C, consists in the evaporation of physical adsorbed water; Step 2, between 160 and 210 °C, results from the decomposition of GO functional groups; Step 3, between 210 and 300 °C, relates to the sulfates contained of Hummers' GO and to aromatic products, such as benzene, indicating that the carbon sheets could be decomposed at such low temperature, while previous studies reported this decomposition occurs above 350 °C. Moreover, we discovered that Step 3 is an endothermic process, which has not been revealed in literature, because such step is often shadowed by the strongly exothermic decomposition reactions of Step 2.

Reduced graphene oxide (rGO) is a dense graphene-like material. Nevertheless, by addition of KOH (potassium hydroxide), a degradation process could be activated at high temperature (e.g. at 700 °C), so that a large quantity of pores are generated in the basal carbon networks, thus obtaining a material that in principle could be used for membrane applications. The activation energy of this process is calculated to $E_a = 179 \pm 2$ kJ/mol. When the mass ratio of GO:KOH changes from 1:1 to 1:5, the BET surface area could increase up to 625 m^2g^{-1}. However, when a higher amount of KOH was added (GO:KOH=1:7 and 1:10), the GO sheets would be seriously damaged, resulting in the decrement of BET surface area.

The introduction of KOH and the high-temperature treatment make rGO brittle and reduce its adhesion on substrate, thus preventing the possibility to use such materials for preparing membranes. Therefore, we developed a new nanocomposite material by mixing GO with poly allylhydridopolycarbosilane (AHPCS), as this polymer is converted into porous SiC by pyrolysis at temperature > 700 °C. After thermal treatment, the composite has BET specific area of 49 m^2g^{-1}. In addition, this fabricated GO+AHPCS nanocomposite could stack on the substrate tightly and form a continuous and integrated membrane with the hydrophilic property (contact angle = $50^o \sim 69^o$). This membrane has also a very high thermal resistance and retains its integrity as well after calcination at 300 °C for 30 min in air. This GO+AHPCS composite has great potential to be applied for membrane researches.

DANSK RESUME

Grafenoxid (GO) er et fantastisk materiale, der er en oxideret form af grafen. GO er anvendt i mange forskningsområder såsom vandrensningsmembraner, sensorer, halvledere, medicin bærere og katalysatorer på grund af dets unikke todimensionelle struktur (enkelt-atom-tykt lag) og fremragende egenskaber (f.eks. høj molekylær selektivitet). Målet med dette PhD projekt er at undersøge den strukturelle og kemiske udvikling af GO under varmebehandlinger og udforske potentialer af reduceret GO (rGO) materialer i membrananvendelse.

Den termiske reduktionsmekanisme og kinetik af Hummers' GO blev studeret. Reduktionsprocessen af GO kan inddeles i 3 step gennem lavtemperatursbehandling. Step 1, under 160 ℃, består af fordampning af fysisk adsorberet vand. Step 2, mellem 160 og 210 ℃, resulterer af dekomponering af GOs funktionelle grupper. Step 3, mellem 210 og 300 ℃, relateres til sulfat indeholdet af Hummers' GO og til aromatiske produkter (såsom benzen, indikerende at carbon ark kunne blive dekomponeret ved så lav temperatur, selvom tidligere arbejde har rapporteret over 350 ℃). Derudover opdage we at Step 3 er en endoterm proces, hvilket ikke er vist i tidligere litteratur, fordi sådan et step ofte er skygget af den stærke exoterme dekomponeringsreaktion i Step 2.

Reduceret grafeneoxid (rGO) er en dens grafen-lignende materiale. Ved at tilsætte KOH (kalium hydroxid) kan degraderingsprocessen alligevel blive aktiveret ved høj temperature (ved 700 ℃), så et stort antal porer bliver dannet i det basale carbon netværk, og dermed opnås et materiale, der i princippet kunne blive anvendt som membran. Aktiveringsenergien af denne proces er beregnet til E_a = 179 ± 2 kJ/mol. Nå vægtforholdet GO:KOH ændres fra 1:1 til 1:5, stiger BET overflade arealet op til 625 m^2g^{-1}. Når højere mængder af KOG tilføjes (GO:KOH=1:7 og 1:10), bliver GO arkene alvorligt beskadiget, hvilket formindsker BET overfladearealet.

Introduktion af KOH og højtemperaturs behandling gør rGO skørt og reducerer dens klæbning på substrater og dermed forhindres muligheden for at bruge sådan et materiale til at lave membraner. Derfor udviklede vi et nyt nanokomposit materiale ved at blande GO med poly allylhydridopolycarbosilane (AHPCS), da denne polymer omdannes til porøs SiC ved pyrolyse ved temperaturer > 700 ℃. Komposittet har et BET specifikt areal på 49 m^2g^{-1} efter termisk behandling. De fabrikerede GO+AHPCS nanokompositter kunne stables stramt på substratet og forme en kontinuer og integreret membran, der beholder den hydrofile egenskab (kontaktvinkel = $50^o \sim 69^o$). Denne membran har også en meget høj termiskmodstand og beholder dens integritet efter kalcinering ved 300 ℃ i 30 min i luft. Dette GO-AHPCS komposit har et stort potentiale til membranforskning.

ACKNOWLEDGEMENTS

This thesis has been submitted to the Faculty of Engineering and Science, Aalborg University for assessment in partial fulfillment of the PhD degree. The thesis is based on the submitted or published scientific papers which are listed in Section 1.3. The PhD study was started from February 2016 to March 2019. The work was primarily conducted at the Section of chemistry at Aalborg University. The study was financed by both China Scholarship Council and Aalborg University.

First of all, I want to give my heartfelt gratitude to my supervisor Professor Yuanzheng Yue. Three years ago, I met great frustration in abroad studying. He provided timely help to me and offered me an opportunity to study in his research group. It made me come to Denmark for pursuing my PhD degree in 2016. Under Yuanzheng generous guidance, I truly enjoyed my PhD study and could dominate my research independently.

Secondly, I would like to thank my second supervisor Associate Professor Vittorio Boffa. He is a nice and kind teacher with his unique filled Italian passion. Vittorio has brought me into the fantastic world of 2D materials. His ardent encouragement motivate me to roam in the ocean of graphene science. I benefited a lot from him.

I also acknowledge Professors Hong Jiang and Changjiu Li from Hainan University in China, who made the recommendation for me to come to Denmark for this degree. My cooperators Professor Haizheng Tao (Wuhan University of Technology), Luca Maurize and Professor Giuliana Magnacca (University of Turin) deserve to be appreciated for involving in various measurements.

My kind acknowledgements also go to my dear colleagues at Aalborg University: Donghong Yu, Hao Liu, Nerea Mascaraque, Katie Kedwell, Katarzyna Janowska, Ang Qiao, Martin Bonderup Østergaard, Chao Zhou, Sonja Haastrup, Xianzheng Ma, Kacper Januchta, Rasmus Rosenlund Petersen, Cejna Anna Quist-Jensen, Laura Paraschiv, Usuma Naknikham, Qiang Tao, Tobias Kjær Bechgaard, Sheng Li, Pengfei Liu, Chengwei Gao, Jiayan Zhang, René Mossing Thomsen, Malwina Stępniewska, Anil Kumar Suri, Morten Mattrup Smedskjær, Lars Wagner Städe, Henriette Casper Jensen, Anne Flensborg and Lisbeth Wybrandt for great assistance in the lab.

Furthermore, my heart belongs to my parents forever. They give me great support when I made the decision of studying abroad. Without their love and encouragement, I could not achieve such success so far.

The last but not least, I must appreciate myself. The road of science is not easy, you never know what is waiting for you in front. Numerous failures? Frustrated heart? Endless lonely exploration? I am glad that I make through the PhD period and can sing out now, ‘Yes, I make it!’

Thanks all!

TABLE OF CONTENTS

CHAPTER 1. INTRODUCTION

1.1. BACKGROUND AND CHALLENGE

The 21st century has been termed as the Century of Energy and Environment [1,2]. Under the accelerated development, human being's sanitation is greatly improved along with the world population's rapid growth; industrial expansion constantly spring up, accompanied by explosive energy consumption and global climate change. Environment issues are becoming obligatory task for governments and scientists. There are currently many emerging new technologies dealing with the energy concerns. Among the different strategies, 2D materials (two-dimensional) have triggered increasing interest, because of their unique structures and unusual properties, for energy and environmental applications [3,4].

2D materials are usually quite different from those traditional 3D compounds. The 2D materials are normally composed of one atom thick or one polyhedral thick planar sheet [5–7]. Among the big 2D materials family, graphene is the first discovered class in 2004 [8]. Graphene-based materials are comprised of single-atom-thick carbon planes with layered van der Waals heterostrucutres [9]. They have many special properties: great flexibility of layer structure [3], outstanding electronic properties [10], impermeability to all gases [11–13]and excellent mechanical properties [14]. Because of these extraordinary properties, graphene-based materials have been widely studied in many areas, encompassing drug deliveries, photocatalysts, transistors, semiconductors, sensors and separation membranes [15–19].

Graphene Oxide (GO), which contains hydroxyl, epoxide, carbonyl and carboxyl functional groups on the carbon network surface [20,21], is an oxidized version of graphene, as shown in Figure 1-1. Normally, GO is synthesized from graphite by using strong oxidants, e.g. H_2SO_4 and HNO_3 [22–24]. The ratio of C:O could reach 1~4. After the addition of these functional groups, the immanent carbon sheets would become insulator.

With the similar graphene-like structure, one of the most attractive features of GO is that these functional groups could be easily removed from GO through chemical or thermal reduction methods to convert the GO into graphene, while the fabrication of graphene is very expensive. The reduced GO (rGO) is considered to be an applicable intermediate for graphene-based products for industrial scale [25–29]. Various reduction techniques, such as reduction via gases (H_2), high vacuum treatment and pH modification, have been utilized for obtaining highly reduced GO [30–34]. However, the reduction mechanism of GO is still not clear since many functional groups are involved in the reduction process. The chemical evolution of these functional groups and the structural transmutation of the graphene layers remain elusive. Indeed, a number of papers have discussed about GO reduction, however, most of them mainly

concentrate on the high temperature reduction (> 200 ℃). To the best of our knowledge, rather limited amount of studies deal with the low temperature decomposition processes of GO (between 100 and 200 ℃). Besides, such studies usually only focus on the chemical changing and thermal stability, but the thermal kinetics of GO thermal reduction processes has rarely been discussed

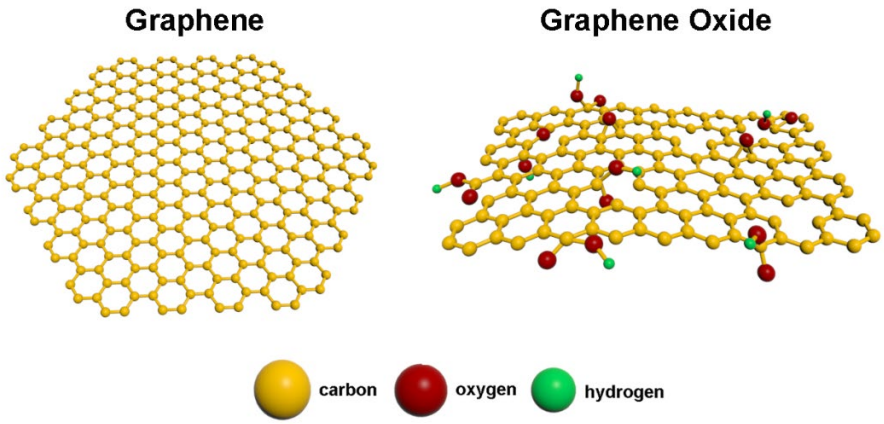

Figure 1-1. Schematic of grpahene and graphene oxide.

Table 1-1. Overview of main properties of graphene-based materials [35–37].

Graphene-based materials	Synthesis Methods	C:O ratio	Electron Mobility ($cm^2V^{-1}s^{-1}$)	Production Cost
Graphene	• Chemical vapor deposition • Thermla decomopsition of SiC • Graphite exfoliation	No oxygen	10000-50000	Very high
Graphene Oixde	Oxidation and exfoliation of graphite	1 ~ 4	insulator	Low
Reduced Graphene Oxide	Thermal or chemical reduction of graphene oxide	8 ~ 246	0.05-200	Low

Besides being the intermediate for graphene production, GO material possesses its own unique properties. The other attractive feature of GO is that its interlayer distance expands to 0.70 nm from 0.34 nm of graphite [38]. Moreover, the existence of the functional groups turns lamellar carbon into hydrophilic so that GO would allow water to be adsorbed into layers. Thus, this behavior could be applied in water separation technologies [39–44]. Some previous studies prove that GO membrane has high selectivity, which is impermeable to all standard gases and only let water molecule go through[45–48]. However, the functional groups could hinder the H_2O transport between the graphene channels because of the hydrogen bonding reaction [49,50]. Furthermore, the GO nano-channels could be easily destroyed at high temperatures due to the instability of the functionalities and/or the hydration of ions in aqueous solutions [51,52]. Hence, GO membranes need to be improved concerning their chemical and thermal stability for practical permeation applications.

Therefore, it is crucial to reveal the GO reduction mechanism for achieving higher stability of GO membranes and for designing the membranes comparable to ultrafiltration or nanofiltration. A detailed understanding of the influence of functional groups and structural disorder on the nano-channels width and defects concentration in the GO deserves to be explored.

1.2. OBJECTIVES

The aim of this PhD project is to investigate the GO structure at different scales, the connection between disorder structure and honeycomb hexagonal structure, and the feasibility of GO films with quantitative control of the oxygen-containing moieties. A variety of characterization techniques will be employed, including Raman spectroscopy, FTIR spectroscopy, XRD, XPS, TEM, chemical stability test, water adsorption test and other relevant techniques. We expect to explore the mechanisms of the GO structural evolution, which could help us fabricate highly permeable and selective GO membranes through a simple and amenable to scale-up method. The objective of this thesis are:

- Investigate the different functional groups of GO and their chemical/physical interactions;
- Provide a detailed study of the mechanisms of the low-temperature thermal reduction of GO;
- Investigate the connection and influence between the disorder in carbon network and the perm-selectivity and mechanical stability of GO membranes;
- Find suitable methods to fabricate GO membranes and to quantitatively and qualitatively control their disorder;
- Investigate the connection and influence between the disorder in carbon network and the perm-selectivity and mechanical stability of GO membranes.

1.3. THESIS CONTENT

The experiments in this thesis were done at Aalborg University, University of Turin and Wuhan University of Technology. This thesis consists of an overview of three main experiments, which would be written into 3 journal papers (either published or submitted for publication). The papers are listed below and will be cited by their roman numerals in the following thesis:

I. Yang Shen, Vittorio Boffa, Ingrid Corazzari, Ang Qiao, Haizheng Tao and Yuanzheng Yue, Revealing Hidden Endotherm of Hummers' Graphene Oxide During Low-Temperature Thermal Reduction. *Carbon*, 138, 337-347 (2018).

II. Yang Shen, Luca Maurizi, Giuliana Magnacca, Vittorio Boffa and Yuanzheng Yue, Nanoporous Reduced-Graphene Oxide for Membrane Application. (to be submitted)

III. Yang Shen, Xianzheng Ma, Vittorio Boffa and Yuanzheng Yue, Porous Nanocomposite Reduced-Graphene Oxide Membrane for Water Filtration. (to be submitted)

CHAPTER 2. EXPERIMENTAL

In this chapter, the synthesis methods and the characterization tests of graphene oxide (GO) and related membrane materials are presented.

2.1. SYSTHESIS

All the chemicals used for the synthesis were purchased from Sigma-Aldrich, unless specified. Graphene Oxide is not a stoichiometric material, so all the mentioned weight ratio below is mass ratio.

2.1.1. GRAPHENE OXIDE

The raw graphene oxide powder was synthesized through Hummers method [23,31,53], whose different steps are shown in Figure 2-1. 92 mL H_2SO_4 (sulfuric acid, 98%), in a 1 L beaker was placed in an ice bath for 10 min first to let it cool down. Then 2.0 g graphite (Graphit Kropfmühl GmbH) was dropped to the beaker and were stirred for 10 min. Later, 2.0 g $NaNO_3$ (99%) was added. After obtaining a homogenous dispersion, 12.0 g K_2MnO_4 (99%) was added slowly to avoid a sudden temperature increase. After 20 min stirring, the beaker was moved to a water bath at 35 ℃ for 1h and a thick dark green paste was obtained. The water bath temperature was increased to 90 ℃ and 160 mL deionized water was poured into the suspension very slowly in order to prevent an uncontrolled temperature increase. After 30 min stirring, the mixture color turned into dark brown. Then, 400 mL deionized water and 12 mL 30% H_2O_2 solution were added dropwise, the suspension's color became light yellow. This initial graphene oxide suspension was washed with 200 mL HCl (5%) one time and 500 mL deionized water 5 times to remove redundant K^+, Mn^{2+} and sulfates. The cleaned graphene oxide (GO) slurry was transferred to pear flask and freeze-dried for 48 h. The dried, yellow and fluffy GO powder was obtained.

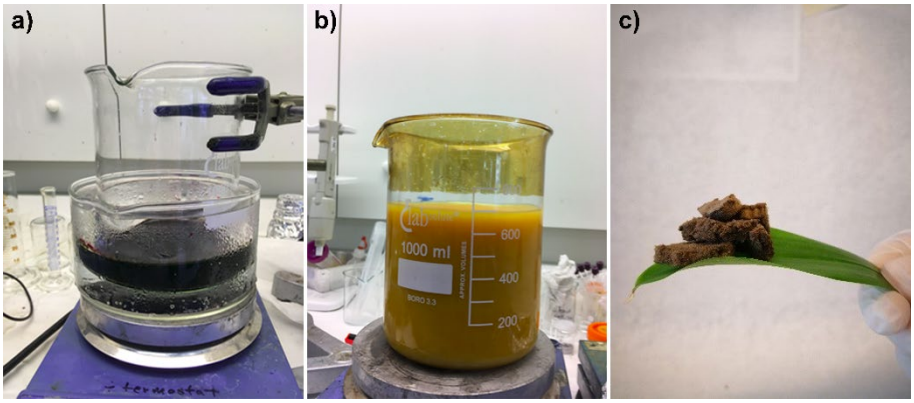

Figure 2-1 Photos of the synthesis process of graphene oxide. (a) The mixture of H_2SO_4, $NaNO_3$ and graphite in ice bath. (b) The graphene oxide suspension. After addition of deionized water and H_2O_2, the dark mixture turn into bright yellow. (c) The dried, brown and fluffy GO powder on a piece of leaf.

All the GO samples were collected from similar concentration dispersion based on the same synthesis and washing procedures. The off-the-shelf GO powders would be used for chemical property analysis and membrane fabrication.

For the thermodynamic experiment (Chapter 3), the raw GO powders were heat treated at 120, 140, 160, 180 and 200 ℃ for different durations (0.5, 1, 3, 7 and 24 h) in Argon atmosphere at the rate of 10 ℃/min.

2.1.2. NANOPOROUS GRAPHENE OXIDE MEMBRANES

0.2 g raw graphene oxide powders were dissolved in 200 mL deionized water and a brown solution was formed. Then, different amount of KOH (86%) powders were added into the solution, the mass ratio of GO:KOH is 1:0.5, 1:1, 1:3, 1:5, 1:7 and 1:10. After stirring 12 h to homogenize the distribution of GO flakes and potassium ions, the solution became black. These samples were ultra-sonicated in water for 30 min. The purpose of ultra-sonication process is exfoliating the GO layers and letting K^+ deposited on GO plane sufficiently. Later, the GO+KOH solution were divided into two groups. The first group of solution was dried at 40 ℃ in air for 48 h until water evaporated mostly. The dried mixture was annealed at 200 ℃ at first to remove the extra H_2O and functional groups of GO in case of sharp reaction and explosion during the TG measurement. Some of the pre-reduced samples were then used for thermodynamics analysis in Ar atmosphere (see details in Characterization part). The left pre-reduced samples were annealed at 700 ℃ for 1 h to apply to other characterizations, for example, X-ray diffraction. The second group of solution was applied to membrane fabrication. 1x1 cm^2 SiC substrates were dipped in different solution for 30 s and then dried for 24 h at room temperature. 3 samples were prepared

for each solution. The membrane samples were annealed at 700 ℃ for 1 h at the rate of 1 ℃/min in Ar atmosphere to produce porous GO membranes.

2.1.3. POROUS GRAPHENE OXIDE COMPOSITE MEMBRANES

First, 10 and 30 mg raw GO powders were dropped into 10 g THF (Tetrahydrofuran, 99.9%), respectively. Then, different amount of AHPCS polymer (Allylhydridopolycarbosilane, 100%, Starfire Systems) were added into the suspension, the ratio of AHPCS:GO is 100:1, 10:1, 1:1 and 0.5:1. The suspension samples were ultra-sonicated in water at room temperature for 1 h to exfoliate the GO layers and homogenize the solutes. The samples were divided into two groups. The first group was put in ceramics crucibles and annealed at 700 ℃ directly for 1h at the rate of 5 ℃/min in Ar atmosphere. The obtained samples were used for characterization, for example, N_2 adsorption measurement. The second group was used for membrane fabrication. Through drop-casting, 100 μL suspension were dropped on 1x1 cm^2 SiC substrate. 2 substrates were coated for each ratio. After drying 24 h at room temperature in air, the samples were annealed at 700 ℃ for 1h at the rate of 1 ℃/min in Ar atmosphere.

2.2. CHARACTERIZATIONS

2.2.1. DIFFERENTIAL SCANNING CALORIMETRY (DSC)

Differential Scanning Calorimetry (DSC) and Thermogravimetry (TG) measurements were performed on a Simultaneous Thermal Analyser 449C Jupiter (Netzsch, Germany).

For thermodynamic experiment, around 4.5 mg pre-treated GO powders were weighted in a platinum crucible at room temperature. The initial temperature was set at 40 ℃, then increased temperature to 600 ℃ at a rate of 10 ℃/min in argon atmosphere. To exclude the heating rate's effect on thermal data's accuracy, the original GO and 160 ℃-24h samples were picked to perform the DSC measurements with the same operation steps at heating rate of 5 K/min and 15 K/min. The isobaric heat capacity curves for each measurement were calculated relative to a reference sapphire sample of comparable mass (25 mg). The enthalpy of the calorimetric peaks was determined by using the software NETZSCH Proteus Thermal Analysis. Isothermal gravimetric measurements were also performed to calculate the activation energy. GO samples of ~ 4.5 mg were weighted in alumina crucible at room temperature, then set temperature heated to the target temperature (120, 140, 160, 180 and 200 ℃) at a rate of 40 ℃/min and held on for 24 h in Ar atmosphere.

For GO+KOH experiment, suitable amount of samples (depends on the ratio, normally sample covers 2/3 of crucible) were weighted in platinum crucible at room temperature. The initial temperature was set at 40 ℃, then increased temperature to

1000 ℃ at a heating rate of 15 ℃/min in Ar atmosphere. Sapphire reference sample (25mg) was also measured to calibrate the calculation of each sample. In isothermal gravimetric measurements, different ratio samples were tested at 600, 700 and 800 ℃ for 5 h in alumina crucible in Ar atmosphere, respectively.

2.2.2. FOURIER TRANSFORM INFRARED SPECTROSCOPY (FTIR)

Fourier Transform Infrared Spectroscopy (FTIR) analysis was performed by using Varian 660-IR spectrometer (Agilent, USA) at room temperature. Raw GO powders grinded with dried (at 100 ℃ in oven for over 24 h in air) KBr powders (99.5%, Merck) under the ratio GO:KBr = 1:200. GO composites (GO+AHPCS) used the same ratio with KBr as the raw GO powders. Then, pellets of each sample were prepared for FTIR tests. The scan range was 4000-400 cm^{-1}. All the samples were repeated 3 times to reduce error.

2.2.3. X-RAY PHOTOELECTRON SPECTROSCOPY (XPS)

X-ray Photoelectron Spectroscopy (XPS) was performed by using ESCALAB 250Xi spectrometer (ThermoFisher Scientific, USA) with Al Kα radiation. We tested C1s and O1s spectrum at pass energy of 50 eV. The spectra were calibrated by referencing the binding energy of carbon (C1s, 284.6 eV). The data was fitted by using PeakFit software.

2.2.4. ELEMENTAL ANALYSIS (EA)

Based on XPS data, besides carbon and oxygen, Elemental Analysis was carried out to detect other kinds of element, in order to predict the by-products. Around 5 mg GO sample were tested by using Series Ⅱ CHNS/O Analyzer-2400 (PerkinElmer, USA) at room temperature. Each group of sample was measured 3 times for error reduction. The average value was chosen as the final data.

2.2.5. RANMAN SPECTROSCOPY

Raman spectra were recorded on an Invia Raman microscope (Renishaw) with the wavelength of 532 nm. In case of the reduction of GO samples, a typical power of 0.1W energy laser was used. The scan range was 150-3000 cm^{-1}. Every sample was tested 3 times for error reduction.

2.2.6. X-RAY DIFFRACTION (XRD)

X-ray diffraction (XRD) measurements were performed by using XRA 888/D (PANalytical, Netherlands) with Cu Kα radiation in the range of $5^o < 2\theta < 40^o$. Before testing, all the samples were grinded into powders for a better resolution. The

calculation of graphene oxide interlayer distance was based on Bragg's equation: $2d \sin\theta = n\lambda$ [54,55].

2.2.7. TIME-RESOLVED INFRARED SPECTROMETRY - THERMOGRAVIMETRY – MASS SPECTROMETRY (FTIR-TG-MS)

To test the chemical evolution of GO powder with temperature changing, a Time-Resolved Infrared Spectrometry – Thermogravimetry - Mass spectrometry (FTIR-TG-MS) combined instrument was used. Around 2 mg GO powders were weighted in platinum pan and 30 ℃ was set as initial temperature. Then heated to 700 ℃ at the heating rate 20 ℃/min in N_2 atmosphere in the Pyris TG part (PerkineElmer, USA). During the thermal test, the released gas was pumped through a pressurized transfer pipe (Redshift S.r.l., Italy) and delivered to FTIR part (Spectrum 100, Perkin Elmer), equipped with a thermostatic conventional gas cell. The data of evolved gas was collected by FTIR continuously in the range of 4000-600 cm^{-1}. The data was analyzed by the Spectrum software (Perkin Elmer). Temperature-resolved infrared profiles of each single moiety desorbed from samples were obtained from the intensity of a representative peak of the investigated species. Besides the FTIR part, Mass Spectrometry (Clarus 560S, Perkine Elmer, USA) in selected ion recording (SIR) mode was also applied to analysis some organic products (for example, benzene, stryrene, naphthlene and phenanthrene), which released during the thermal measurement. For the MS measurement, GO samples were heated from 30 to 400 ℃ at heating rate of 20 ℃/min in N_2 atmosphere. This temperature range covered the selected organic molecules' boiling temperature (Benzene: 80.1 ℃, Stryrene: 145 ℃, Naphthlene: 218 ℃, Phenanthrene: 340 ℃).

2.2.8. PYROLYSIS - GAS CHROMATOGRAPHY - MASS SPECTROMETRY (PRY-GC-MS)

As FTIR-TG-MS results proved the existence of organic products, a higher sensitivity Pyrolysis-Gas chromatography–Mass Spectrometry (Pyr-GC-MS) measurement was applied to explore the evolution of these organic molecules. A CDS Pyroprobe 1500 (Analytical Inc., USA) filament pyrolyzer was connected to the 6890N Network GC system (Agilent Technologies, USA) and the 5973 Network Mass Selective Detector (Agilent Technologies, USA). A methylphenyl-polysiloxane capillary column (30 m, 0.25 mm i.d., 0.25 µm film thickness) was used in the GC system. Around 20 mg GO samples in the pyrolyzer was heated to 300 ℃ at the heating rate of 50 ℃/min and thermal treated at the target temperature for 30 second. He gas was used as the carrier gas at the gas flow of 1.0 mL/min, and the split ratio was 1/20 of the total flow. The tested range of mass spectra was 40-600 m/z under electron impact at 70 eV. All instruments were controlled by Enhanced Chem Station (ver. 9.00.00.38) software.

2.2.9. N_2 ADSORBTION MEASUREMENT

Liquid Nitrogen adsorption were performed by using Micromeritics ASAP 2020 Plus Physisorption (USA). Around 25 mg GO sample was used each time. Before the measurement, the sample was kept at 250 ℃ for 1 h in vacuum to degas the water and impurities. After that, the N_2 adsorbtion measurements were conducted at 77 K. The relative surface area was calculated through the Brunauer-Emmett-Teller (BET) method.

2.2.10. SCANNING ELECTRON MICROSCOPE (SEM)

The morphology of membrane samples were characterized by using scanning electron microscope (1540 XB, Zeiss) at 10 kV. All membrane samples were coated with Au before testing.

2.2.11. TRANSMISSION ELECTRON MICROSCOPE (TEM)

The reduced porous graphene oxide sheets were characterized by using high resolution transmission electron microscope on JEOL 3010-UHR (Nanolab Technologies, USA). The porous sheets were ultsonicated for 30 min before measurement to exfoliate the stacked graphene layers.

CHAPTER 3. GRAPHENE OXIDE THERMODYNAMIC AND REVEALING OF ENDOTHERMAL PROCESS

Graphene Oxide (GO), which has a high concentration of hydroxyl, epoxide, carbonyl and carboxyl functional groups inside, is an oxidized version of graphene [20]. Through different methods, which involve chemical or thermal reduction, these functional groups could be removed, thus converting GO to a graphene-like structure [25–28]. Therefore, GO can be considered as an inexpensive and easy-to-process precursor of graphene-based materials. As the low-temperature thermal reduction of GO is the easiest method for large scale industrial production of graphene-based materials, investigation of the mechanism of GO thermal reduction process is very important. In reason of that, many previous studies have discussed about GO thermal reduction [25,30–33]; however, most of them mainly concentrate on GO reduction at the relative high temperature (above 200 ℃). On the contrary, only a limited number of paper has explored GO decomposition process at low temperature (between 100 and 200 ℃). Besides, such researches often only focus on the thermal stability and structure changing of GO, while the thermal dynamic and kinetics of GO reduction processes during annealing seldom has been discussed. Here, we study about the mechanism and the thermal dynamic of GO reduction process between 120 and 200 ℃. We prepared the starting GO from natural graphite, by applying the Hummers' method, as this is the most common way of preparing GO. We attempt to provide a reasonable commentary for the GO low temperature thermal reduction [1].

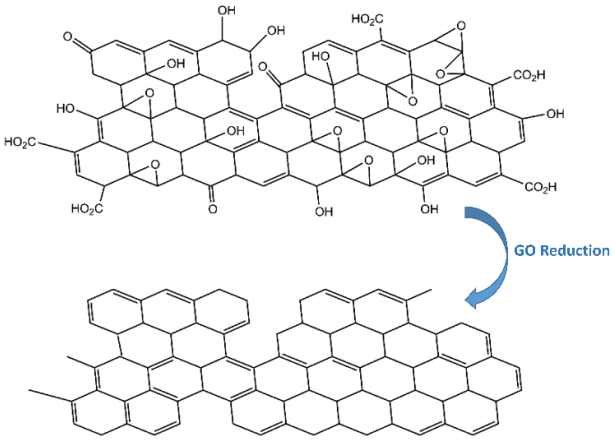

Schematic 3-1. From Graphene Oxide to Graphene.

[1] Results in this chapter have been published in Paper I.

3.1. GO THERMAL REDUCTION PROCESSES

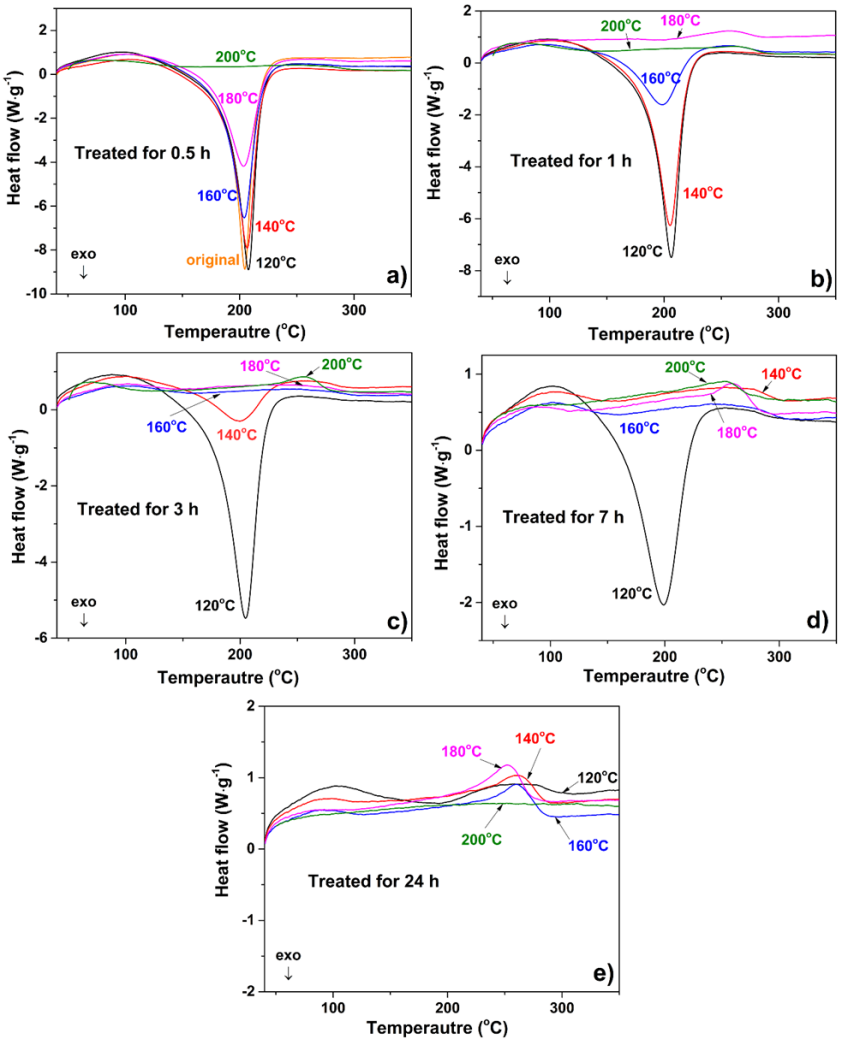

Figure 3-1. DSC data of all graphene oxide samples under 5 different annealing durations at different temperature.

The raw GO powders were pre-heated at 120, 140, 160, 180 and 200 ℃ in argon atmosphere for 0.5, 1, 3, 7 and 24 h. The DSC data of all GO samples with same annealing time at different temperature are showed in Figure 3-1. In Figure 3-1(a), there is an exothermic peak around 210 ℃ of the original GO sample, which starts from 100 and ends at 250 ℃. By increasing annealing temperature, the exothermic peak area decreases gradually to almost disappear when the temperature reaches

200 ℃. For longer annealing duration, for example for 3 h (as shown in Figure 3-1(c)), the exothermic peak area decreases sharply. The heat flow of 120 ℃-0.5 h starts form -9 W/g, while 120 ℃-3 h sample's heat flow starts from -5.5 W/g. Besides, for 3 h annealing, the exothermic peak disappears at much lower temperature 160 ℃. In Figure 3-1(d), only 120 ℃-7 h sample shows the exothermic peak. When the annealing time extends to 24 h, the exothermic peak of all pre-heated GO samples are totally disappeared. However, with the vanishing of exothermic peak, an endothermic peak shows up obviously. In Figure 3-1(c), this endothermic peak already appears in the curve of 200 ℃-3 h. For annealing 7 h (Figure 3-1(d)), the presence of the endothermic peak starts above 180. If GO samples been heated for 24h, all data have the endothermic peak, except 200 ℃-24 h sample, of which the curve is nearly flat.

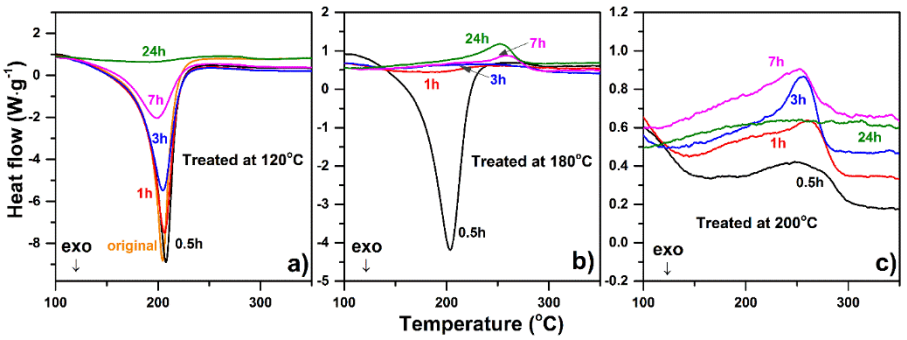

Figure 3-2. DSC data of 3 groups of GO samples at same temperature with different annealing duration: (a) 120 ℃, (b) 180 ℃, (c) 200 ℃.

To explore the GO thermal reduction process more comprehensively, the relation of exothermic peak and different annealing time are also analyzed, as shown in Figure 3-2. 120, 180 and 200 ℃ pre-heated GO samples are picked. The exothermic peak in Figure 3-2(a) is quite similar to the one in Figure 3-1(a). The original GO sample shows an exothermic peak centered at 210 ℃. At 120 ℃, the peak is fading with the annealing time increasing. After 24 h, the exothermic peak is totally disappeared even at such low temperature. When the GO heat treated at 180 ℃, only 0.5 h annealing sample shows the exothermic peak and the1 h annealing sample's curve is almost flat. For 180 ℃-24 h GO sample, a small endothermic peak shows up. In Figure 3-2(c), after annealing at 200 ℃, no matter how long the heating duration is, there is only endothermic peak in the curve, except the flat 200 ℃-24 h GO curve. In conclusion, time and temperature are two key factors of GO thermal reduction process. Longer annealing duration or higher heating temperature could both facilitate the reduction reaction.

For many of the DSC curves in Figure 3-1 and 3-2, a clear exothermic peak and/or a small endothermic peak could be observed in the temperature range of 100~300 ℃ depending on the annealing temperature and time. To further confirm that these two

peaks concern distinct reactions, Dynamic Thermogravimetric Analysis is used. The TG data of all pre-heated GO samples are showed in Figure 3-3. The original GO samples has the similar mass loss curve with 120 ℃-0.5 h sample, so it is not depicted here. In Figure 3-3(a), at 120 ℃, three distinct mass loss steps could be observed, so called Step1, Step 2 and Step 3. Based on the TG curves, each step has a specific temperature range, that for Step 1 is 100~160 ℃, for Step 2 is 160~210 ℃, for Step 3 is 210~300 ℃.

For different annealing time and temperature, these steps show various mass loss. At 120 ℃ (in Figure 3-3(a)), the related mass loss of 120 ℃-3 h of Step 1,2 and 3 are 12.31%, 17.86% and 9.18%, respectively. With the annealing time increasing, from 3h to 24 h, the mass losses of Step 1 and Step 2 decrease sharply, especially the disappearance of Step 2 is very evident. However, the mass loss of Step 3 does not change much: it is normally around 10% for all samples at 120 ℃. At higher annealing temperature, e.g., 140 and 160 ℃ (as shown in Figure 3-3(b,c)), the three steps' mass loss show the same trends the these TG curves: the mass loss of Step 1 and 2 gradually decrease to nearly 0%, while only Step 3 remained. When the annealing temperature increases to 180 ℃ (Figure 3-3d), after 24 h, the mass loss of Step 3 slightly reduces to 7%. 200 ℃ thermal treated data are showed in Figure 3-3(e) to explore the decrement of Step 3. At 200 ℃, the mass loss of Step 3 still keeps 10% below 1 h annealing. With longer heating duration, the Step 3 mass loss starts to decrease. For 7 h annealing, around 4.52% Step 3 left. In 200 ℃-24 h sample's curve, the Step 3 totally vanish away.

To show the mass loss tendency more clearly, the mass loss data of all samples are collected, as shown in Figure 3-4 ($\Delta m/m_0$ is the relative mass loss, Δm is the mass loss, m_0 is the initial mass related to the pre-heated GO sample). For Step 2, as 200 ℃ pre-heated GO samples do not have this step, there is no 200 ℃ annealing data in Figure 3-4(a). The relative mass loss of Step 2 decreases slowly with the annealing time at 120 ℃. With the temperature increasing, the slope of the lines in Figure 3-4(b) becomes larger. At 180 ℃, the Step 2 reaction occurs quickly in less than 3 h. For Step 3, the 160 ℃ curve changes little and remains horizontal from 0.5 to 24 h. The relative mass loss results of 120 and 140 ℃ annealed GO samples are not showed in Figure 3-4(b) as they are similar to 160 ℃ curve. The mass loss of them keep at 10% and would not change as a function of the annealing time. On the contrary, the 180 ℃ curve in Figure 3-4(b) shows a negative slop. For samples annealed at 200 ℃, the mass loss associated to Step 3 decreases quickly from 10% to nearly 0% after 24 h annealing.

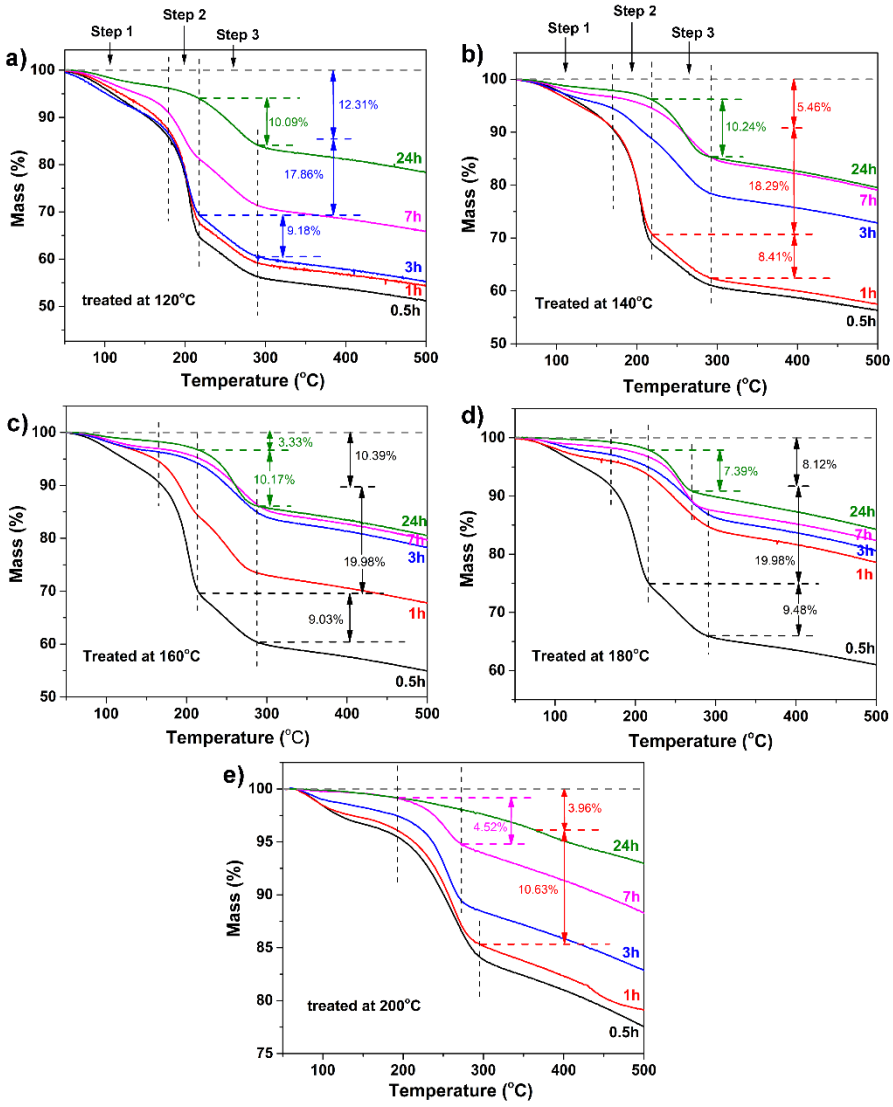

Figure 3-3. TG data of annealed GO samples at same temperature with different annealing duration. The horizontal grey dash lines are used as baseline, set as mass=100%. The vertical dotted lines are used for visual. The data of original GO are similar with 120℃-0.5h sample, for simplicity, it is not showed here.

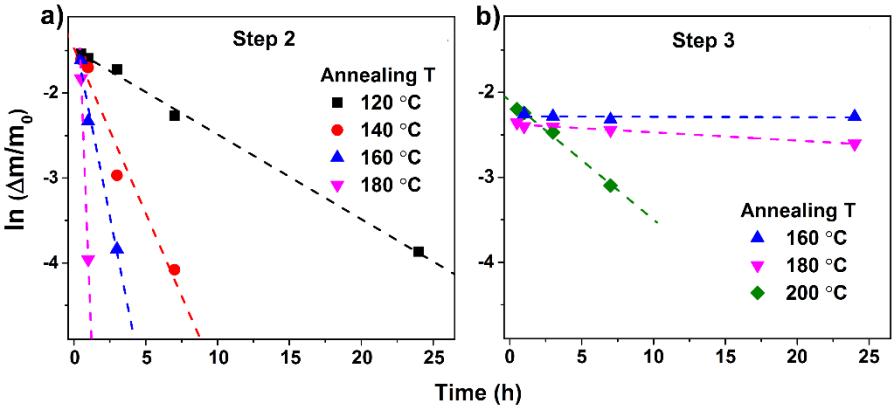

Figure 3-4. TG data of annealed GO samples. The dotted lines are linear fits. (a) Mass loss of Step 2, (b) Mass loss of Step 3.

In the above DSC and TG discussion, an exothermic peak or an endothermic peak could be observed in different thermal treated GO samples in DSC figures, while three different mass-loss steps: Step 1,2 and 3 are detected in TG data. In some samples, for example, annealed at 120 ℃ (Figure 3-2(a) and Figure 3-3(a)), there is a big exothermic peak at first in DSC curve, and 3 distinct steps show up in TG. With the heating time increasing, the exothermic peak decreases, meanwhile, the mass loss of Step 1 and 2 also decreases progressively. Besides, when the endothermic peak shows up, e.g. Figure 3-2(b), there is only Step 3 left (Figure 3-3(d)). At 200 ℃ annealing, the endothermic peak starts to fade in Figure 3-2(c), at the same time, the mass loss of Step 3 decrease gradually. Here comes 3 questions:

(1) What are the exact mechanisms of the three distinct reaction steps?

(2) If Step 2 response to exothermic peak, Step 3 is related to endothermic peak, why there is no endothermic peak for low annealing temperature samples (like 120 ℃)?

(3) Are Step 2 and Step 3 concerted reactions or they are independent?

To explore these questions, the DSC curves of 3 representative pre-heated GO samples are picked: the original GO sample, 160 ℃-1 h and 160 ℃-24h samples, as shown in Figure 3-5.

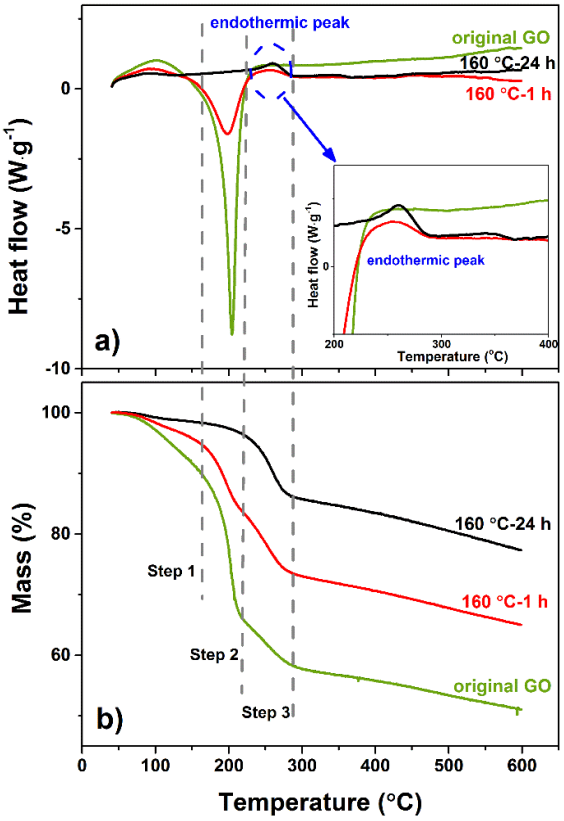

Figure 3-5. DSC and TG data of 3 picked GO samples: original GO, 160 ℃-1 h and 160 ℃-24h. The dashed are used for visual.

In Figure 3-5, the original GO curve presents the typical DSC and TG profiles: a big exothermic peak in the temperature range of 100~250 ℃ in DSC curve, 3 distinct reaction steps in TG figure in the same temperature region. Based on former literature: Step 1 (below 160 ℃) is normally on account of evaporation of physical absorbed and nano-confined water [56]. Step 2 and 3 reactions (between 160 and 300 ℃) are due to the decomposition of the functional groups on the carbon plane of GO [31,57–60]. Above 300 ℃, there is no peak response in DSC, while TG shows very small mass loss. This is mostly ascribed to the degradation of GO carbon network [61]. As this high temperature degradation has no DSC response, it would not be discussed in this chapter. As expected, after annealed at 160 ℃ with different duration (1 h and 24 h), the mass loss of Step 2 decreases progressively, while the mass loss of Step 3 remains the same. As consequence of a lower mass-loss during Step 2, the exothermal response drops gradually. No mass loss or exothermic response are detected for Step 2 in the 160 ℃-24 h sample. Therefore, this sample shows only the mass loss and the endothermic peak corresponding to Step 3 in the temperature range between 210 and

300 ℃. Despite the original GO and 160 ℃-1 h do not show a clear endothermic peak in this temperature range, their TG curves show the same mass loss as observed for 160 ℃-24 h. Thus, we could infer that the intense exothermic peak of Step 2 covers the small endothermic transition of Step 3 in the samples annealed at low temperature.

To examine the influence of the heating rate on Step 1, Step 2 and Step 3 characteristic temperatures, the original GO and 160 ℃-24 h samples are additional measured in DSC-TG at the heating rate of 5 and 15 ℃/min, as shown in Figure 3-6. Three distinct steps could still be observed in Figure 3-6(b). As expected, the reaction temperature slightly shift to higher value from 5 to 15 ℃/min. Nevertheless, the Step 2 is never observed for 160 ℃-24 h. On the contrary it is always observed the endothermic peak corresponding to Step 3 (Figure 3-6(c)(d)). These data indicate that heating rate does not have an effect on the appearance of the 3 reaction steps.

In above DSC-TG data, we find an endothermic transitions (Step 3) in the temperature between 210 and 300 ℃. Such transition is hidden by the large exothermic peak of GO thermal reduction (Step 2), unless samples are annealed at T >160 ℃. As Step 2 has a different reaction temperature zone with Step 3, we deduce that the two processes are decoupled. The thermal reduction process of Hummers' GO is usually considered as a single exothermic event, and therefore most of the previous researches ignored the endothermic transition, which was revealed in this work.

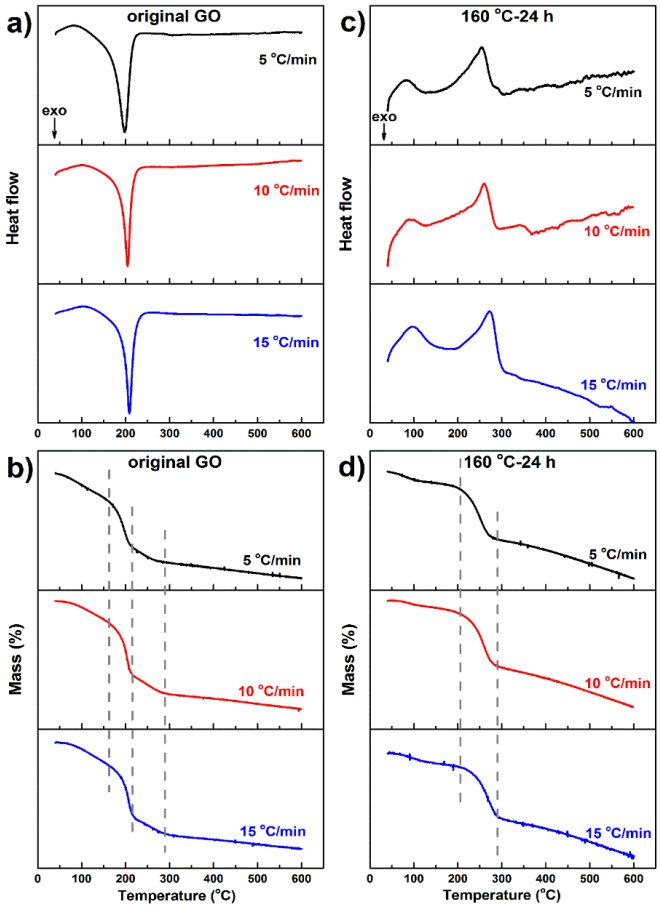

Figure 3-6. DSC and TG curves of original GO and 160 °C-24h samples at different heating rates. The vertical dashed line are used for visual.

3.2. GO REDUCTION THERMODYNAMICS

In Section 3.1, different annealed GO samples are measured in DSC-TG. Three distinct reactions steps, which is respective related to exothermic or endothermic peak, could be observed. Following those phenomena, Isothermal Gravimetric Analysis is used for investigating the different reaction mechanisms, as shown in Figure 3-7. The ρ (X-coordinate) is the fractional mass loss based on the original GO.

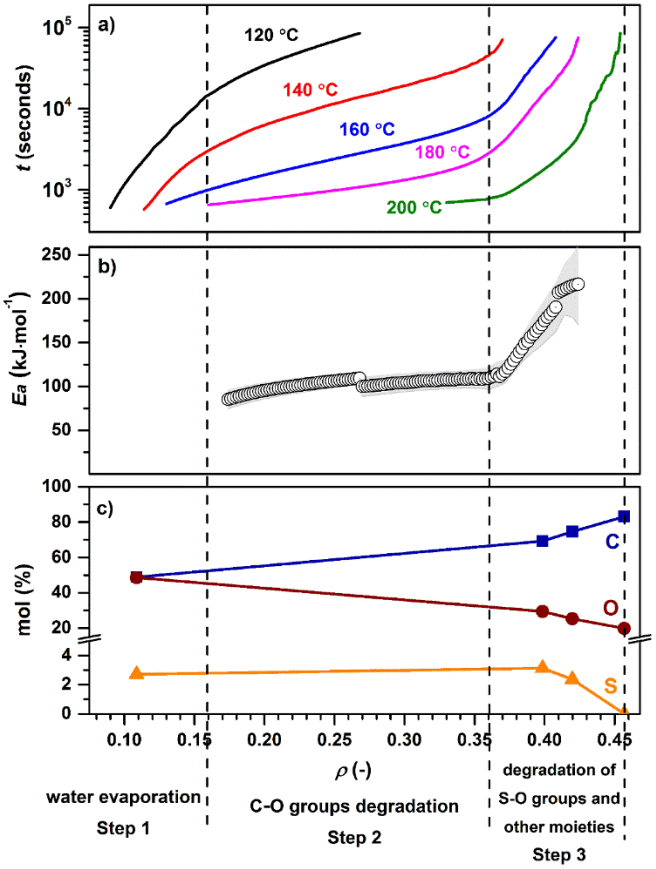

Figure 3-7. Isothermal Gravimetric Analysis of all pre-heated GO samples. (a) The isothermal TG curves. (b) The calculated activation energy. (c) The content tendency of samples during 3 reaction steps.

In Figure 3-7(a), the original GO sample are tested in TG at 5 different temperatures for 24 h. The curves show the relationship between time t and degree of degradation ρ. The 5 isotherms profiles present different slops. The slopes' transitions are mainly at two specific mass loss values: ρ = 0.16 and ρ = 0.36. Thus the different decomposition steps are divided based on these two ρ values, which corresponds to Step 1, Step 2 and Step 3. Through the figure, a good agreement of mass loss could be observed between the isothermal test and dynamic thermogravimetric measurement (in Figure 3-5). Hence, we could indicate that $\rho \leq 0.16$ corresponds to Step 1, which is related the vaporization of water in GO, and $\rho > 0.16$ corresponds to Step 2 and Step 3, which is associated with degradation of functional groups. Obviously, at 120 ℃, the degradation of GO is much more slowly than at 200 ℃. For higher temperature, the fractional mass loss is larger.

In Figure 3-7(b), the relative activation energy E_a is calculated based on the isothermal results by using the MacCallum method [62,63]. The equation can be expressed as follow:

$$t = f(\rho) \cdot A \cdot exp(^{E_a}/_{RT}) \quad \text{Eq. 3-1}$$

Where t is the degradation time; R is the universal gas constant; A is the pre-exponential factor; $f(\rho)$ is set as an undefined function of the GO reduction.

The curve in Figure 3-7(b) is E_a vs ρ. At the beginning, in the fractional mass loss range $0.16 < \rho \leqslant 0.36$, the activation energy is nearly constant, $E_a = 112 \pm 6$ kJ/mol. When in the range $0.36 < \rho < 0.45$, the activation energy abruptly increased sharply. At last test point, $E_a = 248 \pm 9$ kJ/mol. This trend could be explained by the fact that at first the most liable functional groups are decomposed (Step 2) during the thermal treatment. Thermal degradation of the most stable moieties (Step 3) has higher activation energy and therefore occurs at a higher temperature.

In order to understand (1) what is exactly occurred during Step 3, (2) what is the difference between Step 3 and Step 2, Elemental Analysis is done for different pre-heated GO samples. The atomic composition data of samples are shown in Table 3-1 and plotted in Figure 3-7(c).

Table 3-1 Composition of annealed GO samples by using Elemental Analysis. (Relative percent)

Sample	C [at. %]	S [at. %]	O [at. %]	S/C	O/C
120 ℃-0.5h	48.88	2.71	48.41	0.055	0.990
200 ℃-0.5h	69.21	3.13	27.66	0.045	0.400
200℃-3h	74.57	2.36	23.07	0.032	0.309
200 ℃-24h	83.06	0.00	16.94	0.000	0.204
Rewashed GO	43.86	0.14	56.00	0.003	1.276

In 120 ℃-0.5 h sample, which has similar composition with the original GO, the concentration of Carbon atoms is nearly the same of Oxygen atoms' concentration (48.88% C and 48.41% O, O/C = 0.99). Unexpectedly, 2.71% Sulfur is also detected. As a consequence of the partial thermal reduction, in 200 ℃-0.5 h, the percent of C increases to 69.21%, while the concentration of O decreases to 27.66% and the ratio between oxygen and carbon shrinks to 0.40. The concentration of S is slightly increased (about 3%), as a consequence of degradation of the oxygen containing functional groups (e.g. phenols and carboxylic acids). By increasing annealing time

(T = 200 ℃), the percent of C atoms reaches 83.06% and O atoms drops to only 16.94% (200 ℃-24 h). Besides the loss of oxygen atoms, the atomic concentration of S atoms decreases to 0% for 200 ℃-24 h.

Combined with the DSC-TG profiles (as shown in Figure 3-7(c)), it could be inferred that at low temperature (below 200 ℃), during Step 1 and Step 2 ($\rho \leqslant 0.36$), the water desorbs and the most liable functional groups are decomposed so that the O atoms' concentration reduces largely. Meanwhile, the concentration of S atoms keeps at 3%, suggesting that Step 2 does not involve the degradation/desorption of S-containing groups.

For samples annealed at 200 ℃, the percent of S decreases with the annealing time to reach 0 for 200 ℃-24 h. Therefore, the mass loss of Step 3 should be connected to the reduction of S-containing moieties. Considering our GO samples are prepared based on Hummers' method, of which the synthesis process involves the use of concentrated sulfuric acid, there are large quantity of residual sulfates in GO. This type of impurity has also been reported by some former researches [64]. However, based on elemental analysis, even if all the sulfur-moieties are decomposed in the form of SO_2, the calculated mass loss could only reach to 6.2%. Therefore, decomposition of S-containing moieties could not account for the 10% mass loss measured from the data reported in Figure 3-3. Hence, we deduce that some other moieties could be decomposed from GO during Step 3. This reaction step should be related to the decomposition of a complexity of functionalities.

To further confirm the reaction mechanism of these steps, besides the relative activation energy, the enthalpy (ΔH) of each pre-heated GO samples is calculated by using a sapphire reference and plotted in Figure 3-8. In Figure 3-8(a), exponential fittings (based on the equation: $y = a * (1 - e^{-bx})^c$) are used for indicating the trends of the enthalpy value with annealing time changing. From the 5 curves, it could be observed that with longer annealing time, more functional groups are released during Step 2 and less ΔH is measured in GO. For samples annealed at 120 ℃, the ΔH decreased smoothly from -1400 to less than 100 J/g in 24 h annealing time. However, at higher temperature, for example 180 ℃, ΔH of Step 2 decreases dramatically to nearly 0 J/g in a very short annealing duration. At 200 ℃, Step 2's ΔH even could not be detected (around 0 J/g) during the whole annealing duration. In Figure 3-8(b), all samples' Step 2 enthalpy data are collected. A linear relationship could be observed between ΔH and the relative mass loss. By fitting these points, we figure out that the thermal degradation of 1 gram of GO moieties sample would release 6.7 ± 1 kJ energy during Step 2.

Compared with Step 2, the ΔH absolute values of Step 3 are much smaller, as shown in Figure 3-8(c). For samples annealed below 180℃, the data points are mainly distributed in the range $0.16 < \rho \leqslant 0.36$. Only 200 ℃-7 h and 200 ℃-24 h samples' Step 3 ΔH are located in the range $0.36 < \rho < 0.45$. At lower temperature, the Step 3

enthalpy increases with the annealing duration, e.g. 140, ΔH increases from 20 to 67 J/g. At 200 ℃, the Step 3 enthalpy has the same increased tendency in the first half part, when $\rho > 0.36$, the ΔH starts to decrease until 0. Figure 3-8(d) presents the trends more clearly. The points are gathered at 3 zones: Group Ⅰ, Group Ⅱ and Group Ⅲ. The Group Ⅱ is the turning point. To explain these transitions, the activation energy E_a is taken into consideration (in Figure 3-8(c): in the first half part, exothermic and endothermic reactions both exist. With the content of exothermic process decreasing, the content of endothermic process keeps the same, resulting in the higher relative percentage of the endothermic reactions so that the ΔH of Step 3 increases (from Group Ⅰ to Group Ⅱ). Later, only endothermic reactions are left, with longer annealing time at 200, Step 3 starts to degrade and the related ΔH decreases concurrently (from Group Ⅱ to Group Ⅲ). Step 3 is a combination of different kinds of reactions and the combined presence of it is a small endothermic peak. Moreover, combined with the mass loss results, it could be discovered that although with the same mass loss, ΔH absolute values of Step 2 and Step 3 are huge different. For example, in 160-24 h sample, the calculated enthalpy $\Delta H \approx 67$ J/g corresponds to around 10% mass loss of Step 3, while in 160 -1 h sample, the 10% mass loss of Step 2 reveals much larger enthalpy $\Delta H \approx -508.8$ J/g. There are 2 possibilities of this phenomenon: (1) The decomposed functional groups of Step 2 contain more energy than the functionalities of Step 3. (2) As Step 3 is a combination of exothermic and endothermic process, the negative value and the positive value of the enthalpy cancel each other out.

As above discussed, different functional groups are decomposed and appear as exothermic peak or endothermic peak during Step 1, Step 2 and Step3. To prove our results' representativeness and repeatability, we check many literature and find out their TG data also appear the special Step 3 [59,64–72]. Besides, we conclude that the Step 3 only shows up in the GO prepared by Hummers' method. However, in those literatures, most of them ignore of independence of Step 3 and summarize Step 2 and Step 3 as one process. They ascribe this big one step to the degradation of labile and stable functional groups. More importantly, to authors' best knowledge, none of them discovered that Step 3 is an endothermic process.

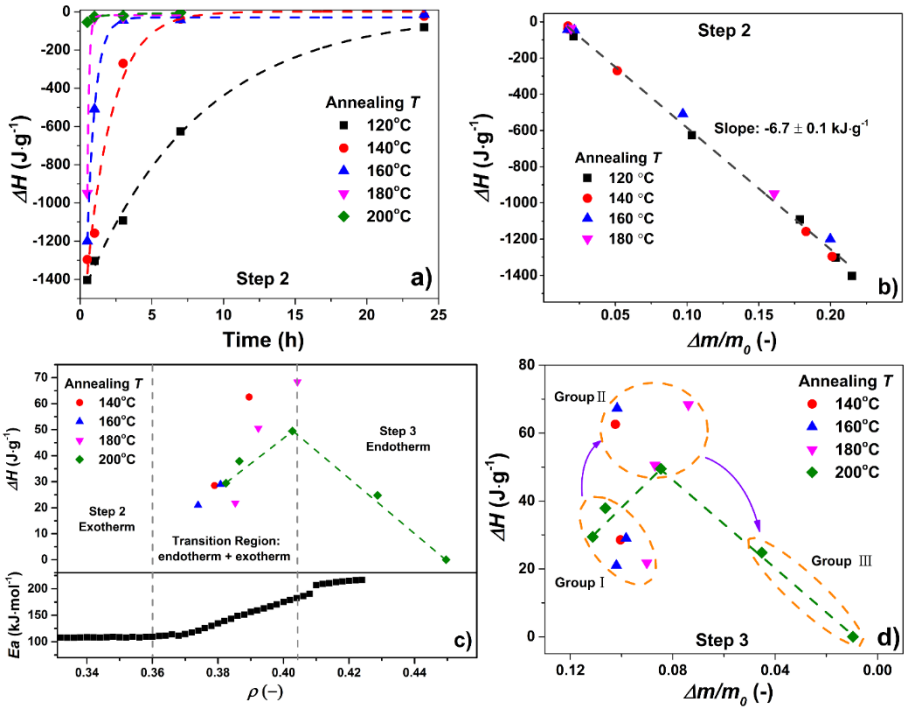

Figure 3-8. The calculated enthalpy (ΔH) of each pre-heated GO samples. (a) ΔH of Step 2 (the exothermic part). The dotted curves are exponential fits. (b) The relationship between mass loss and enthalpy of Step 2. The dotted lines are linear fits. (c) ΔH of Step 3 (the endothermic part). The dotted line is only for visual. (d) The relationship between mass loss and enthalpy of Step 3. The dotted linear line, dashed circles and the arrows are for visual.

3.3. BY-PRODUCTS DURING GO REDUCTION

Two distinct reduction processes, namely Step 2 and Step 3 are confirmed by DSC and TG. With the involvement of elemental analysis, Step 3 is associated to the degradation of sulfates. However, TG analysis suggests that not only S-containing moieties are degraded during Step 3. To gain more information about the gas products formed during the degradation steps, a combined continuous FTIR-TG-MS measurement of the original GO sample is performed. The responses of the MS and FTIR detectors for CO_2, CO, H_2O and benzene are shown in Figure 3-9. Below 160 ℃ (Step 1), only the H_2O curve shows a small peak, which could be ascribed to the evaporation of confined water in GO (the mass loss of Step 1). Between 160 and 250 ℃, a peak appears in the curves of CO_2, CO and H_2O. These peaks are centered at 220 ℃ and cover the temperature range of Step 2. Thus, the mass loss of Step 2 is consistent with the exothermic degradation of oxygen-containing moieties as carboxylic acids, phenols and epoxy groups. On the contrary, SO_2 is detected only in

the temperature zone 220 ~ 300 ℃, where Step 3 located. The release of sulfates is a main part of Step 3 mass loss. The release of sulfates in this temperature range has already been reported [68,70,73] and it could explain a significant part of Step 3 mass loss. However, also benzene molecules are released between 220 and 290 ℃. We infer the appearance of this peak comes from the decomposition of GO carbon basal network. In literature, most researches indicate that the GO carbon plane starts to decompose only at high temperature [61,74], e.g. higher than 350 ℃. On the contrary, our results show that the GO carbon basal plane could degrade temperature as low as 220 ℃.

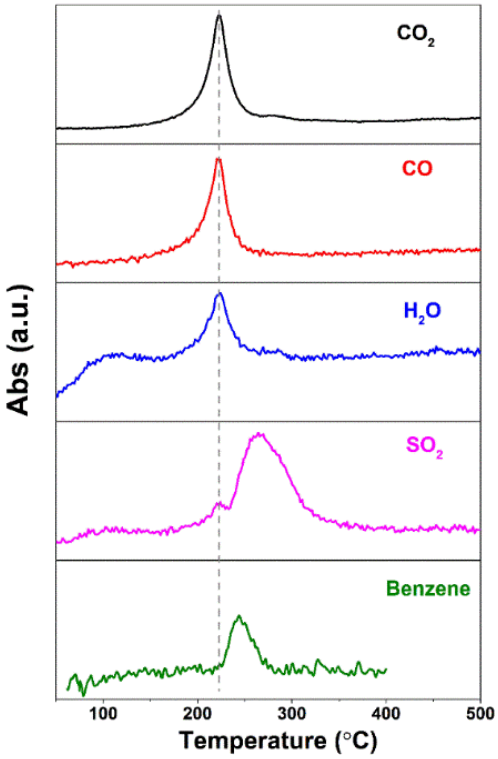

Figure 3-9. Gas developed during thermal treatment of the original GO sample, as revealed by FTIR-TG-MS analysis.

To confirm that the endothermic Step 3 mainly corresponds to the decomposition of sulfur-containing moieties, samples original GO and 160 ℃-24 h samples are washed extra 15 times with deionized water to remove the sulfur impurities (hereinafter these samples are name 'rewashed GO'). Washing process is a widely used method for GO materials to remove the impurities and obtain neater GO samples. The atomic composition of rewashed GO samples are listed in Table 3-1. It shows that the content of sulfur is only 0.14 atom%. TG measurements (Figure 3-10(a)(b)) show that there

is no clear mass loss in Step 3 for both the rewashed samples. The low S content influences the position of the big exothermic peak (Step 2) but not its appearance. In Figure 3-10(c)(d), it is more obviously that the rewashed samples have no endothermic peak corresponding to Step 3. S-impurities are a dominate part of the mass loss of Step 3.

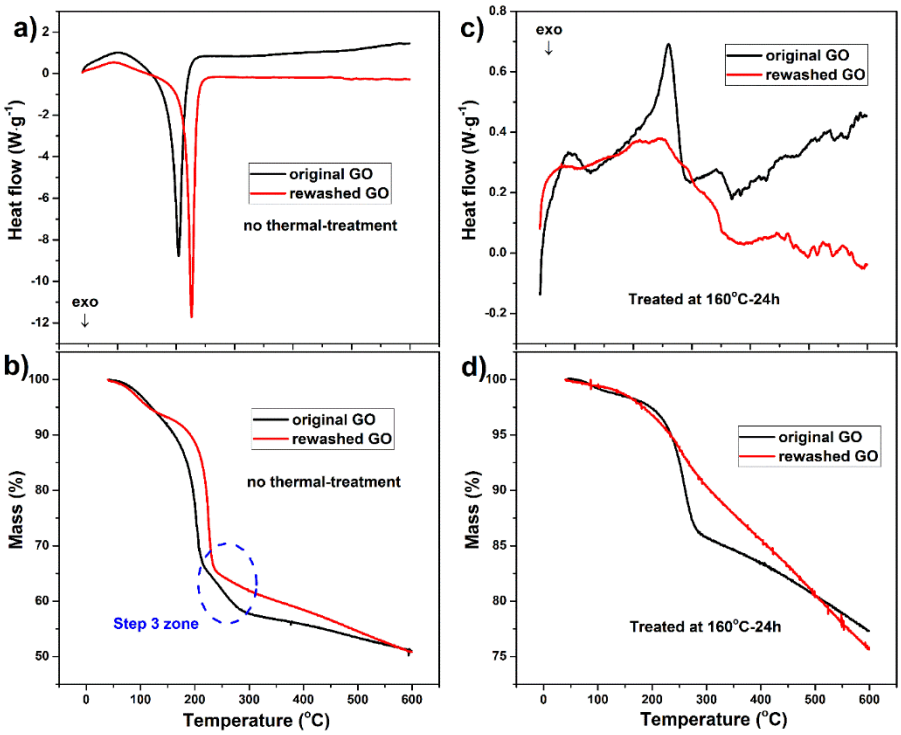

Figure 3-10. DSC-TG results of original GO and 160 ℃-24 h samples and their rewashed samples. (a-b) The original GO and its rewashed samples. (c-d) The 160 ℃-24 h and its rewashed samples.

In addition, as indicated by the Elemental Analysis (Table 3-1), there is around 3.2 atom% of S in the original GO sample. However, this quantity of sulfur could not be account for all the 10% mass loss, measured during Step 3. Furthermore, the release of benzene is revealed in Figure 3-9. Probably, various types of volatile aromatic by-products are released during Step 3. Therefore, to explore the mass loss deficit of Step 3, a Pyr-GC-MS measurement is performed. Three selected GO samples are tested at 300 ℃ for 20 seconds: the original GO, 200 ℃-3 h and 200 ℃-24 h samples, the results are shown in Figure 3-11. Figure 3-11(a) shows the characteristic peaks of 7 aromatic products, detected from the original GO sample, that is, released during Step 1, Step 2 and Step 3: benzene, benzaldehyde, 2-furancarboxyaldehyde, 2,5-furandione, N,N-dimethyl-formamide and styrene. In Figure 3-11(b) (sample

200 ℃-3 h), there are only 3 peaks, which shall arise from Step 3: benzene, benzaldehyde and 2,5-furandione. The disappearance of the signals of the other organic products indicates that the decomposition of functional groups during Step 2 accompanies with the degradation of GO carbon sheets, resulting in structural defects formation. The 200 ℃-24 h sample, annealed for a longer duration, releases only benzene (Figure 3-11(c)). As benzene is always been detected in all three samples, we infer that the generation of benzene does not strongly depends on the species and quantities of the functional groups. Besides, specific aromatic products are released in Step 2, for example, styrene could not be observed in 200 ℃ annealed samples.

Our discovery of aromatic by-products during GO thermal reduction is consistent with some former studies [64,74]. However, in their studies, the annealing temperature is relatively high (above 400 ℃). Our Pyr-GC-MS data shows that a small amount of some specific species of aromatic by-products could be released at lower temperature, that is, the GO carbon basal plane would start to degrade below 300 ℃.

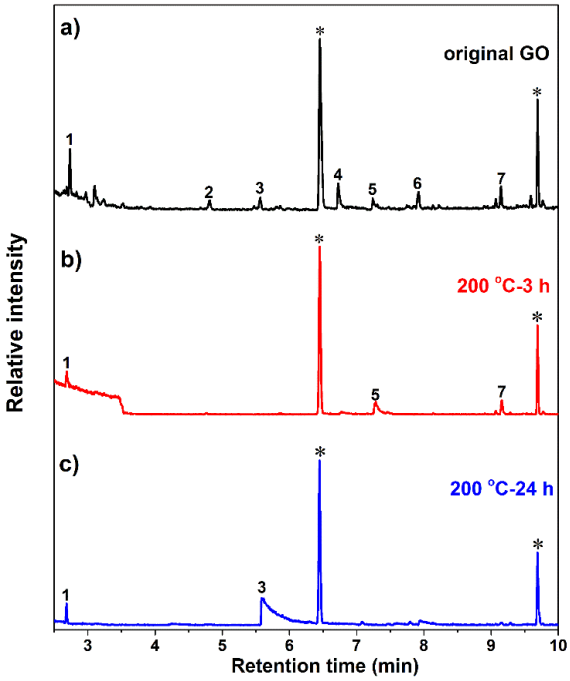

*Figure 3-11. Pyr-GC-MS results of three selected GO samples. Numbers indicate the characteristic peak of: 1. Benzene; 2.Toluene; 3. N,N-dimethyl-formamide; 4. 2-Furancarboxyaldehyde; 5. 2,5-Furandione; 6. Styrene; 7. Benzaldehyde. The marked peaks with * come from the instrument column.*

3.4. STRUCTURE EVOLUTION OF GO DURING THERMAL REDUCTION

After identifying the by-products during Step 1, 2 and 3, the structure evolution of GO during the thermal reduction process is studied as well.

To gain insight of the evolution of GO functional groups during thermal reduction, 2 groups of samples are selected to be analyzed by FTIR: GO annealed at 120 and 200 ℃, the results are shown in Figure 3-12. Peaks at 1050 cm^{-1} correspond to the C-O bond vibration; peaks at 1225 cm^{-1} correspond to C-O-C epoxide bonds; peaks at 1380 cm^{-1} correspond C-OH bonds; peaks at 1620 cm^{-1} correspond to C=C vibration; peaks at 1730 cm^{-1} correspond carboxyls; peaks at 3400 cm^{-1} correspond to hydroxyl groups and intercalated water [58,75,76]. For samples annealed at 120 ℃, the spectral changes mainly correspond to the structural changes of GO in Step 1 and Step 2. In Figure 3-12(a), it could be seen that with for long annealing duration, the peak at 3400 cm^{-1} decreases sharply, because of the evaporation of physical absorbed and nano-confined water. Besides, the peaks of C-O and C-OH (1050 and 1380 cm^{-1}) become less pronounced gradually and disappear for the sample annealed for 24 h, as highlighted by the yellow stripes. The area of the characteristic carboxyls peak decreases as well, but does not vanish after 24 h annealing. The epoxide and C=C peaks (1225 and 1620 cm^{-1}) vary very slightly at 120℃ annealing. In Figure 3-12(b), the normalized absorbance spectra of the samples annealed at 200 ℃ are exhibited. At this temperature, Step 1 and Step 2 occur in less than 0.5 h, so the spectral changes that we could observe in Figure 3-12(b) are connected with Step 3. Similar to the 120 ℃-24 h GO sample, these spectra are characterized by 3 peaks corresponding to the vibrations of carboxyl groups (1730 cm^{-1}), C=C (1620 cm^{-1}) and epoxides (1225 cm^{-1}). After 24 h heat treatment, all three functional groups still could be observed. It indicates that carboxyls and epoxides strongly bond to the GO carbon basal sheet and are not completely degraded even after exposure at 200 ℃ for 24 h, while C=C bond comes from the carbon plane itself. However, the intensity of these 3 functional groups all decrease, especially the carboxyls characteristics peak.

Based on Figure 3-12(b), the relative intensity ratio of 3 peaks are calculated, as shown in Figure 3-13. For a longer annealing time, $I_{C=O}/I_{C=C}$ decreases from 0.31 to 0.14, quite a few amount of carboxyls is decomposed and not many C=O bonds left after 24 h annealing at 200 ℃. It emphasizes the fading of carboxyls peak in Figure 3-12(b). About epoxides, the ratio $I_{C\text{-}O\text{-}C}/I_{C=C}$ decreases form 1.76 to 1.05. A lot of C-O-C are degraded as well, but there are still some amount of epoxides left.

Hence, the mass loss of Step 3 partly results from the decomposition of carboxyls and epoxides. Despite the presence of sulfur in our GO samples, which has been revealed by Elemental Analysis and GC-MS, we could not confirm the band related to sulfates in the FTIR spectra. Normally, the sulfate vibration bands are located at 1183, 1221

and 1417 cm^{-1} [65,68], which happens to are overlapped with the broad epoxides (1225 cm^{-1}) and C-OH (1379 cm^{-1}) peaks respectively.

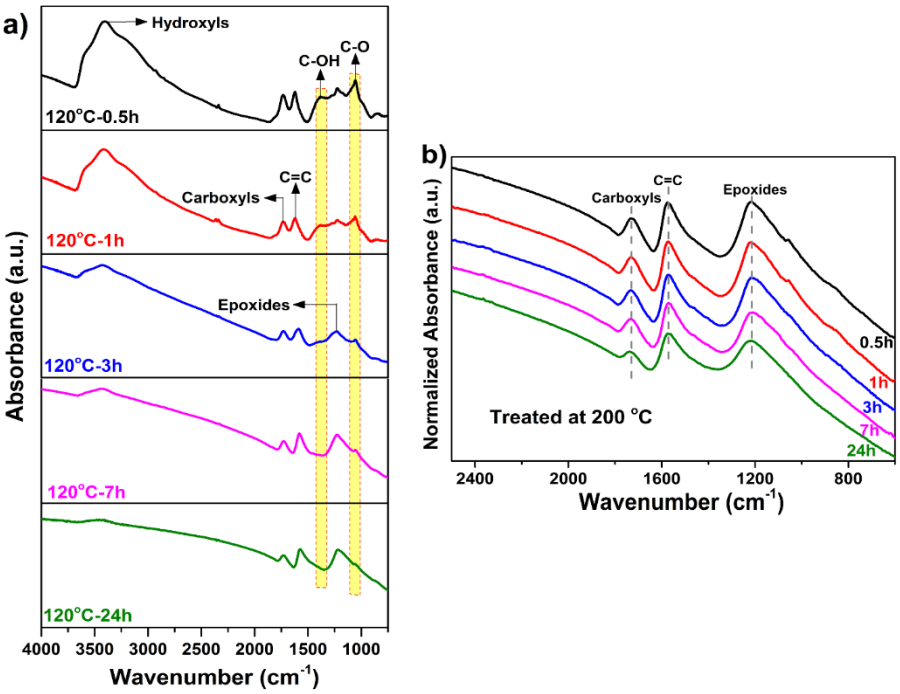

Figure 3-12. FTIR data of 2 groups of annealed GO samples. (a) GO annealed at 120℃. (b) GO annealed 200 ℃.

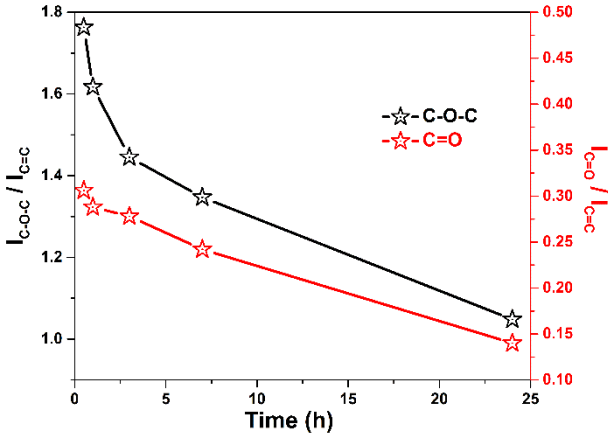

Figure 3-13. The intensity of FTIR peaks of 200 ℃ annealed GO samples.

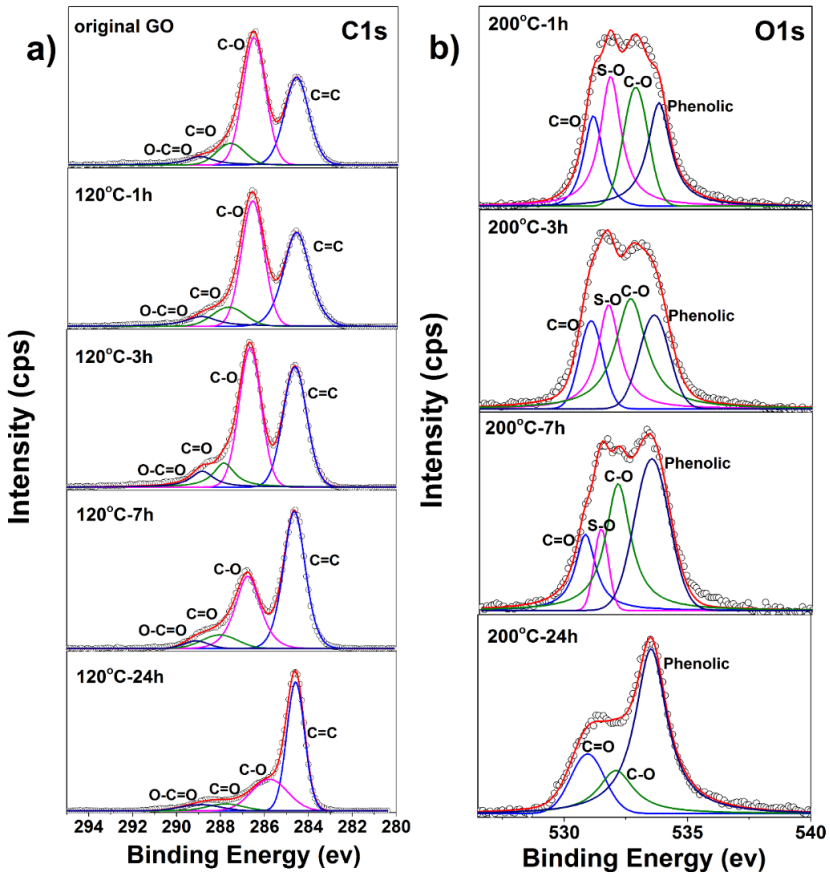

Figure 3-14. XPS data of GO samples. (a) C1s spectra of 120 ℃annealed GO samples. (b) O1s spectra of 200 ℃annealed GO samples.

In order to investigate the evolution of functional groups, especially about the sulfates bonding, original GO, and GO samples annealed at 120 and 200 ℃ are for XPS measurements. The results are shown in Figure 3-14. Figure 3-14(a) reports the C1s spectra. Based on previous literatures [54,77], we fit the XPS curves into 4 peaks corresponding to O-C=O (288.8 ev), C=O (287.8 ev), C-O (286 ev) and C=C (284.6 ev). The relative areas of these fitted peaks are listed in Table 3-2. In original GO sample, the C-O has the most quantities, which is 48.49%, while C=O and O-C=O only occupy 9.98% and 5.42%, respectively. When annealed at 120 ℃ for various durations, the concentration of C-O functional groups decreases gradually from 48.49% to 28.92%. Large amount of CO_2, CO and H_2O are released because of the degradation of C-O, leading to an increment of the concentration of the aromatic carbon (C=C). The concentration of carboxyl (O-C=O) and carbonyl (C=O) groups

do not change much, as they are relatively stable at 120 ℃. This observation matches with the FTIR data (Figure 3-12(a)).

Figure 3-14(b) shows the XPS data of GO samples annealed at 200 ℃. As their C1s spectra are similar to the 120 ℃-24 h sample curve, we present only their O1s spectra here. According to former studies [54,78], the O1s spectra of GO could be fitted to four peaks, which are related to four types of oxygen bonds: phenolic (533.4 ev), C-O (532 ev), S-O (531.6 ev) and C=O (531 ev). The area of these fitted peaks are listed in Table 3-3. For 200 ℃-1 h sample, a broad peak could be observed. After the deconvolution, the quantities of the 4 functional groups are 16.17% C=O, 24.42% C-O, 25.50% Phenolic and 31.91% S-O. Samples annealed for different duration show rather different spectra. From the Elemental Analysis, we already observe that during annealing at 200 ℃, the oxygen and sulfur content of GO is highly reduced. As we could see from Table 3-3, the relative concentration of C=O and phenolic increase during the treatment. Therefore, these groups must be stable under the annealing conditions. On the contrary, the amount of S-O dramatic decline from 31.91% to 0%, which agrees with the Elemental Analysis results. On the other hand, the degradation of sulfur generates the formation of vicinal diols [65], which increases the amount of the Phenolic. The quantity of C-O increases from 24.42% to 37.18% at first, then it drops to 19.00%. We deduce that, at first the decomposition of sulfates leads to an increment of the fraction of C-O; however, after a long annealing time (up to 24h), a large quantity of C-O oxygen has been decomposed, thereby its content fraction decreases gradually.

Table 3-2. The area percentage (atom%) of each functional group peak in fitted XPS Figure 3-14(a).

Sample	C=C	C-O	C=O	O-C=O
original GO	36.11	48.49	9.98	5.42
120°C-1 h	39.98	43.75	9.51	6.76
120°C-3 h	39.8	42.74	10.22	7.24
120°C-7 h	54.35	33.87	8.41	3.37
120°C-24 h	58.41	28.92	6.39	6.28

Table 3-3. The area percentage (atom%) of each functional groups peak in fitted XPS Figure 3-14(b).

Sample	C=O	S-O	C-O	Phenolic
200°C-1h	16.17	31.91	24.42	27.50
200°C-3h	15.91	25.12	37.18	21.79
200°C-7h	16.69	8.87	34.43	40.01
200°C-24h	18.09	0.00	19.00	62.91

The FTIR and XPS results reveal the chemical evolution of functional groups during GO reduction. To study the structural changes of the GO carbon plane during thermal reduction, Raman spectroscopy is conducted for all annealed GO samples, the results are shown in Figure 3-15. Two characteristic signals could be observed: D band (1350 cm^{-1}) and G band (1590 cm^{-1}). Normally, the G band corresponds to the first order scattering of E_{2g} mode of the sp^2 hybridized C atoms, in brief, G band presents the GO carbon basal network' scattering; the D band is from the breathing modes of six-atom rings of sp^3 carbon, in other words, D band is associated with the defect structures which is created by the functional groups [79–82]. The intensity ratio of the 2 peaks (I_D/I_G) could describe the degree of defects in GO [83,84]. In Figure 3-15(a), it could be seen that G band has higher intensity than D band in 120 ℃-0.5 h, I_D/I_G=0.891. With the annealing duration increasing, the intensity D band starts to surpass the intensity of G band. In 120 ℃-24 h sample, the intensity ratio I_D/I_G increases to 1.048. During the thermal reduction process, most functional groups are decomposed, resulting in the breakage of carbon network and generating many defect area, so that the intensity of D band increases and G band area decreases. For GO samples annealed at other temperatures, I_D/I_G shows the similar trend (shown in Figure 3-15(b)(c)(d)). However, when annealing temperature increased to 200 ℃, the intensity ratio of GO samples does not change much with the annealing time increasing, $I_D/I_G \approx 1$. As we discussed above, the mass loss observed while annealing GO at 200 ℃ is mainly associated to the degradation of sulfates to SO_2 (Step 3), which do not results in substantial subtraction of carbon atoms from the GO carbon network.

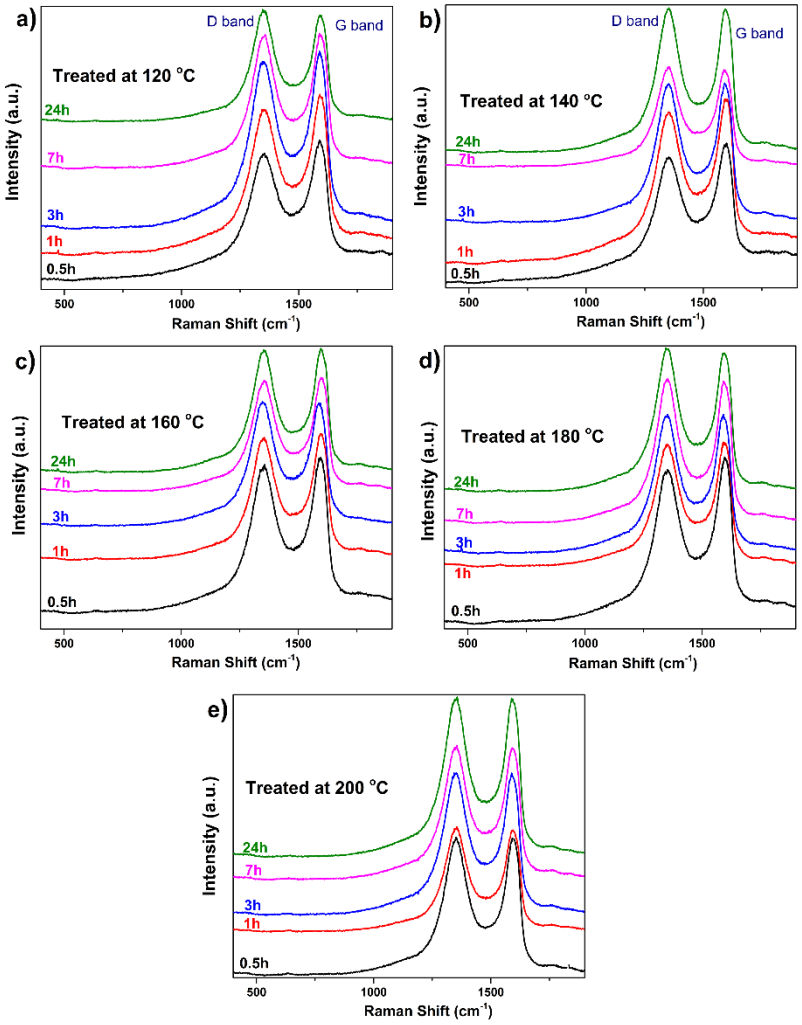

Figure 3-15. Raman spectra of GO samples annealed at 120, 140, 160, 180, and 200 ℃.

Besides the ratio of disorder (defect) and order structure, the crystallographic structures of all annealed GO samples are investigated through X-ray diffraction. The results are shown in Figure 3-16. In Figure 3-16(a), the original GO sample shows a typical sharp peak at 11.28º, which corresponds to a GO carbon sheets' interlayer distance 0.784 nm [30,85–87]. With increasing of annealing time, the peak gradually shifts to higher degree, which means that the interlayer distance decreases, because of the release of the function groups. The peak of the 120 ℃-24 h sample is located at 23.18º, corresponding the interlayer distance decreases to 0.384 nm. The samples

annealed at other temperature present the similar tendency. After the temperature increased to 200℃, there is a broad peak centered at around 23°.

Some of the XRD data are collected in Figure 3-17 to show this trend more clearly. Interestingly, some of the diffractograms present 2 peaks, such as that of 120 ℃-7 h. We mark the 2 peaks as Peak 1 and Peak 2. It could be seen that with an increase of annealing duration or temperature, Peak 1 moves to right step by step until 12.76° (180 ℃-0.5 h), corresponding an interlayer spacing of 0.694 nm. Then, the Peak 1 continues to shift to higher degree, and at 2θ=21.74° a new peak appears (120 ℃-7 h) with an interlayer distance of 0.409 nm. This phenomenon suggests that, at this stage, some carbon domains still contain functional groups and keep the original interlayer distance, while other parts are highly reduced and the layers collapse. Notably, all Peak 2 are somewhat broad, resulting from the large disorder structure. At higher temperature and longer annealing time, Peak 1 moves towards and eventually it is incorporated in Peak 2. In 200 ℃-1h sample, the peak centered at 23.44° and the interlayer distance is 0.380 nm. The combined peak slightly moves to right and ends at 24.57° corresponding to an interlayer distance of 0.362 nm. In the 200 ℃-24 h sample, almost all functional groups have been removed, and some parts of carbon plane are also degraded, as we discussed in the DTA-MS, which leads to many defects, impurities and folding structures so that the Peak 2 is kind of broad.

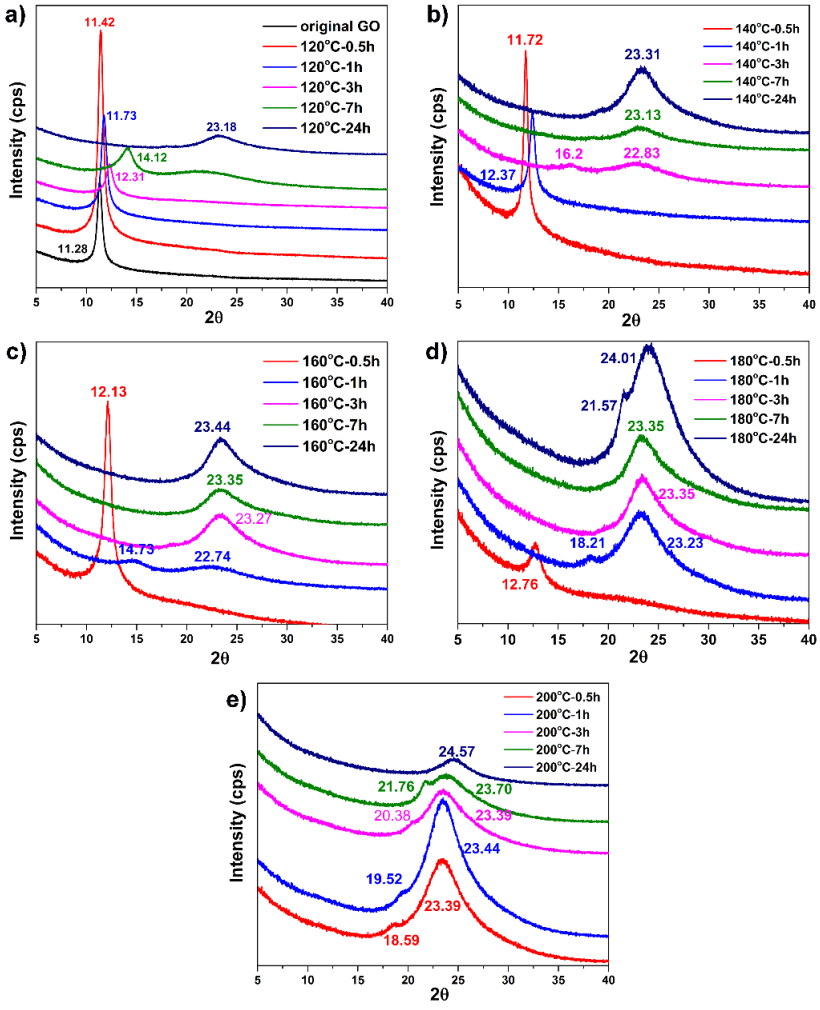

Figure 3-16. X-ray diffraction results of all annealing GO samples. (a) Original GO and annealed at 120 ℃. (b) Annealed at 140 ℃. (c) Annealed at 160 ℃. (d) Annealed at 180 ℃. (e) Annealed at 200 ℃.

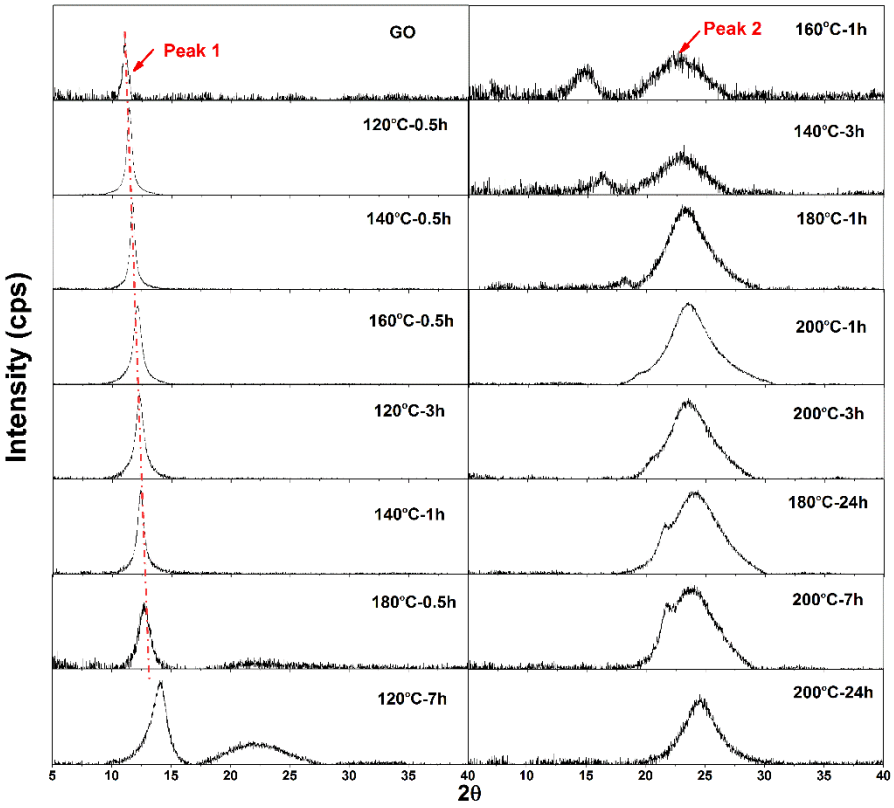

Figure 3-17. X-ray diffraction data of some picked annealed GO. The red dotted line is for visual.

According to some former proposed graphene oxide structure's models and our new findings [45,60,65,88,89], the possible thermal reduction processes (Step 1, Step 2 and Step 3) of the Hummers' GO are here sketched in Figure 3-18.

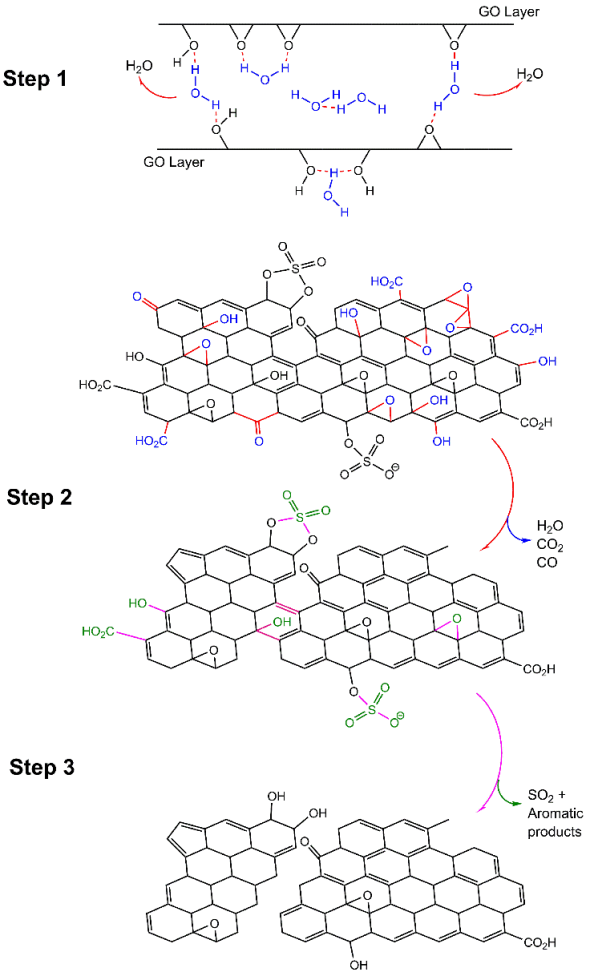

Figure 3-18. Possible thermal reduction process of Hummers' GO.

3.5. SUMMARY

In this Chapter, we investigate the low-temperature thermal reduction of Hummers' GO. Our results suggest that the reduction processes of GO consists of 3 distinct reaction steps: Step 1, Step 2 and Step 3. Below 160 ℃ (Step 1), we observe evaporation of physical adsorbed water; between 160 and 210 ℃ (Step 2), many of the oxygen functional groups are decomposed; between 210 and 300 ℃ (Step 3), sulfates are released. Different steps have various reaction mechanisms. We reveal the Step 3 is an endothermal process, which has never been reported in previous literature. Besides, the chemical and structural evolution during the thermal reduction of GO are explored as well.

CHAPTER 4. NANOPOROUS REDUCED GRAPHENE OXIDE FOR FABRICATION OF MEMBRANES

Graphene oxide (GO) based membranes, with outstanding and eminent water permeability, have attracted great interests in water purification processes, since R. R. Nair et al. reported that graphene oxide membrane is almost impermeable to liquids, vapors and gases, but only allow the permeation of water [45–48,90]. Besides, graphene oxide membrane could be easily fabricated for industrial large-scale production [91]. It has became a rising candidates compared with the traditional filtration methods. However, the neat GO membrane is not thermally and chemically stable and it would be disintegrated in water solution[52,92]. Hence, new types of GO-based membranes need to be developed.

In this study, reduced graphene oxide (rGO) is being explored instead of neat GO, as rGO is much more stable [93,94]. We describe the fabrication of nanoporous reduced graphene oxide (rGO) materials for membrane application. According to the high temperature activation process of alkaline treated carbon materials generating porous structures on carbon networks, KOH is involved here for producing pores on GO carbon planes [34,95]. Such rGO material has highly stability with the similar layer structure as GO. The produced pores would assist the permeation of water.

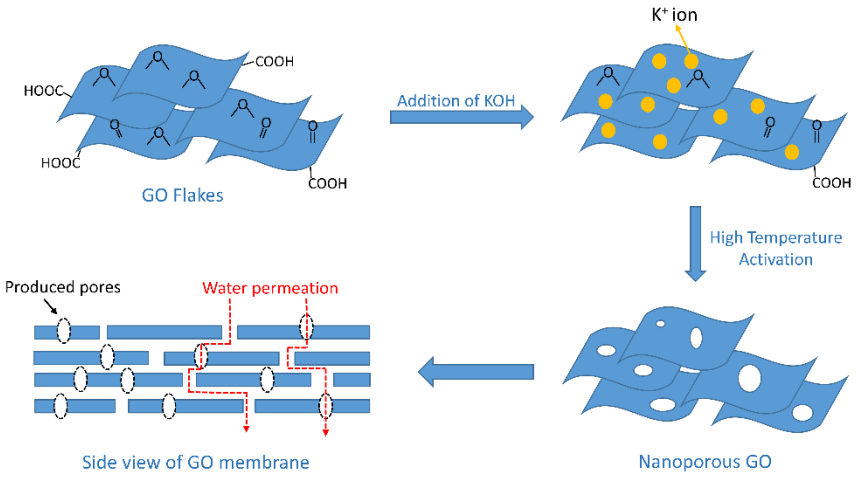

Schematic 4-1. From raw GO materials to nanoporous GO membrane.

4.1. THE ACTIVATION PROCESS

The raw GO samples are mixed with different amount KOH powder, at mass ratio GO:KOH = 1:0.5, 1:1, 1:3, 1:5, 1:7 and 1:10. The mixtures are annealed at 700 ℃ for 1 h in Ar atmosphere. The obtained samples are analyzed by X-ray diffraction, and the results are shown in Figure 4-1. In the XRD curves, we do not observe the reduced GO peak which should be located at around 23° (as we discussed in Section 3.4). Instead, two other main products are detected, K_2CO_3 and K_2O [96,97]. We infer that the by-products stack into the GO interlayers and block the channels and pores, so that the reduced GO could not be seen by XRD.

As we discussed Section 3.1, the reduction process of GO takes place at relative low temperature (below 300 ℃). On the contrary, the activation process by alkalis normally occurs at high temperature (above 600 ℃) [98,98,99]. The potassium ions are dropped on the GO carbon sheets, because of the C strong reducibility, a redox process would happen. In addition to reduction by potassium hydroxide, the carbon atoms in six carbon rings are oxidized to carbonates, resulting in the formation of pores (defects). The related reaction formulas are listed follow[96,100]:

$$6KOH + C \leftrightarrow 2K + 3H_2 + 2K_2CO_3 \quad \text{Eq. 4-1}$$

$$K_2CO_3 + C \leftrightarrow K_2O + 2CO \quad \text{Eq. 4-2}$$

$$K_2CO_3 \leftrightarrow K_2O + CO_2 \quad \text{Eq. 4-3}$$

$$2K + CO_2 \leftrightarrow K_2O + CO \quad \text{Eq. 4-4}$$

To investigate the pristine porous GO XRD curve, 1:3 and 1:7 two samples are selected and been washed with 5% HCl solution to remove the potassium carbonates. The cleaned GO samples are collected and analyzed by XRD. The results are shown in Figure 4-2. A broad peak centered at 25° could be seen in the 1:3 samples, which is similar to the peak observed for rGO. For 1:7 sample, the broad peak is quite weak. Many graphene area have been disintegrated and the disorder structure contributes to the weak amorphous XRD peak.

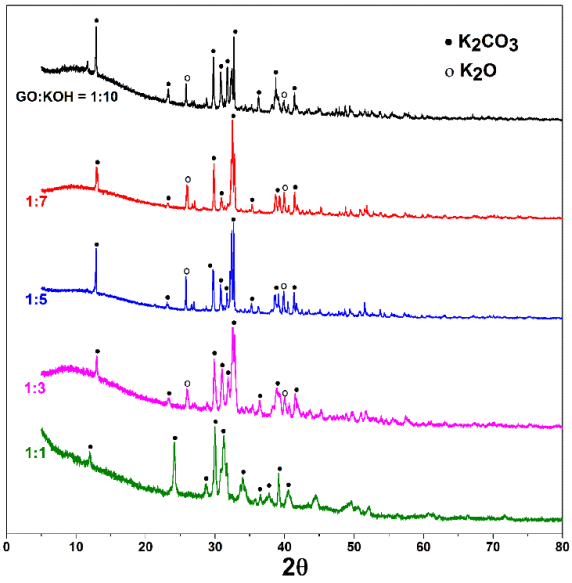

Figure 4-1. X-ray diffraction patterns of GO-KOH samples.

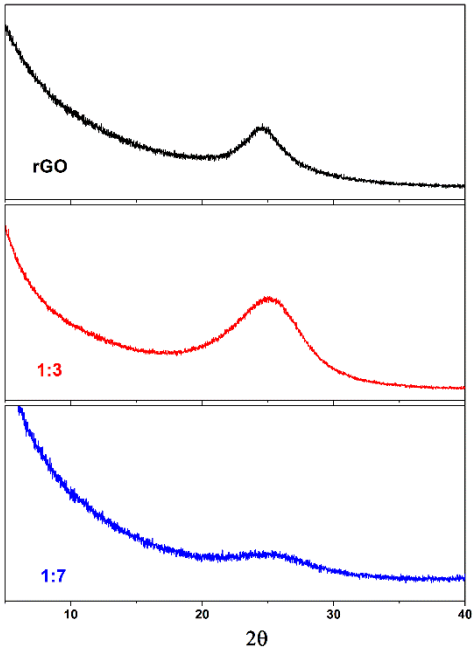

Figure 4-2. X-ray diffraction patterns of washed GO-KOH samples.

4.2. MORPHOLOGY ANALYSIS OF POROUS REDUCED GO

As we discussed in the preceding section, the activation process would largely damage the GO carbon framework. With different amount of KOH, the degree of disintegration varies, resulting in different morphologies in the various samples.

Figure 4-3 shows the appearance of produced samples after washing without grinding or any other physical treatment. The original rGO (reduced GO), without the addition of KOH, presents flake-like shape. During thermal treatment at 700 ℃, GO sheets collapse and stack denser with not much structure destruction. Therefore, the final products are flaky. 1:1 sample still retains the flaky appearance. For 1:3 sample, the GO looks fragmented. With the addition of KOH, because of the redox reaction, GO layer's integrity is greatly broken. More amount of KOH leads to larger GO structure damage. At last, the 1:7 and 1:10 samples are shaggy and powdery. The strong bonding between carbon layers does not tight any more.

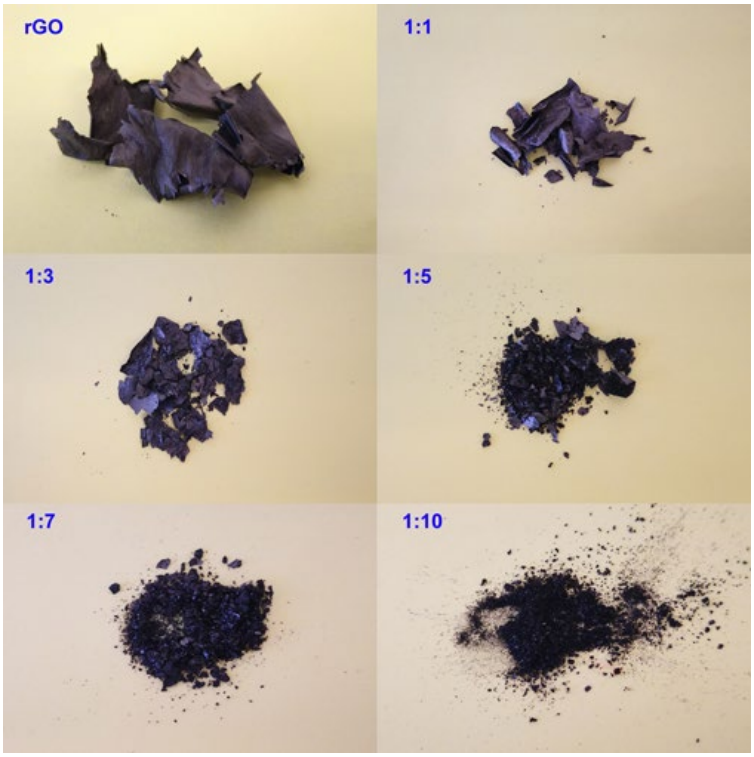

Figure 4-3. Images of porous GO samples without any physical treatment. (a) Reduced GO without KOH. (b) 1:1 sample. (c) 1:3 sample. (d) 1:5 sample. (e) 1:7 sample. (f) 1:10 sample.

To study the difference in microstructure, four samples are chosen for TEM: original reduced GO, 1:1, 1:5 and 1:10. The micrographs are shown in Figure 4-4. In rGO sample, complete and smooth rGO layers could be seen. One such sheet is presented at different magnifications. However, after treatment with KOH, the GO stacks undergo considerable warping and folding. It is very difficult to separate these stacked layers. Hence, in the 1:1 and 1:5 samples, monolayer graphene could seldom be observed. Moreover, the original relative large-size sheet break down into small fragments. In 1:10 sample, the carbon sheets are highly warped. Because of the activation process, the carbon basal plane decomposes and twists, leading to disorder structure, and defects increase. The observation agrees with the XRD results (Section 4.1).

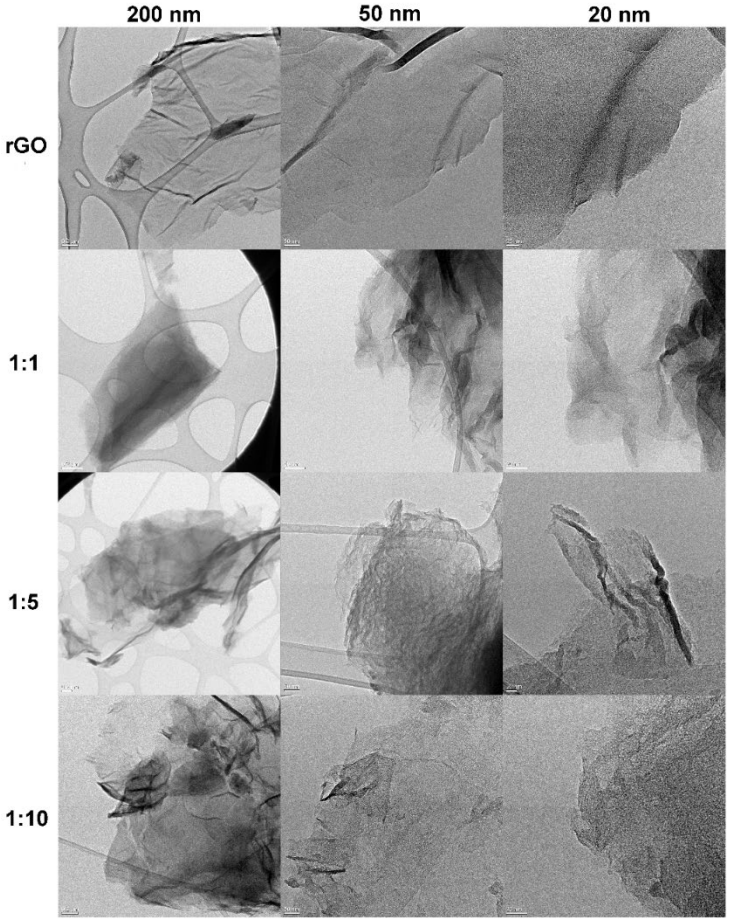

Figure 4-4. TEM images of porous GO samples. Original rGO, 1:1, 1:5 and 1:10 sample under the scale of 200, 50 and 20 nm, respectively.

The N_2 adsorption analysis is carried out to gain information of the porous structure. Five samples: 1.1, 1:3, 1:5, 1:7 and 1:10, are selected for the measurement. The main results of these samples are shown in Figure 4-5 and Table 4-1. Figure 4-5(a) is the isotherms curves of nitrogen adsorbed and desorbed. According to the IUPAC classification [101–103], the adsorption curves of all samples belong to the family type-4 isotherm, because of the appearance of hysteresis loops. At first, with the increase of KOH content, the samples' specific surface area increase remarkably, form 174 to 625 m^2/g (from 1.1 to 1:5 sample). However, with more addition of KOH, the surface area decreases. For example, in 1:7 sample, the BET area reduces to 393 m^2/g. When the ratio of KOH reaches to 10, the prepared sample further decrease to 255 m^2/g, but its value is still higher than that of the 1:1 sample.

The distribution of micropores shows similar trends with surface area, as shown in Figure 4-5(b) and Table 4-1. In 1:1 sample, the volume of micropore is 0.02 cm^3g^{-1}. As more addition of KOH, the micropore volume increases to 0.10 cm^3g^{-1} in 1:5 sample. After that, the micropore volume decreases gradually to 0.06 cm^3g^{-1} in 1:10 sample. However, the volume mesopore and macropore (17< V< 3500 Å) shows an opposite tendency. In 1:1 sample, the meso & macro pore volume is 0.08 cm^3g^{-1}. With increasing amount of KOH, the pore volume increases as well to 0.88 cm^3g^{-1} in 1:7 sample. Unexpectedly, the mesoproe and macropore could not be observed in the 1:10 sample.

From the morphology of the obtained products photos and the TEM images (Figure 4-3 and 4-4), we infer that at first, moderate amount of KOH contributes to the formation of pores in the GO sheets. The porous rGO materials retain a laminar morphology, and have large specific surface area at the same time. However, when the GO is treated with excessive amount of KOH, the carbon network is seriously damaged and the graphene sheets undergo fragmentation, so that the BET area and the micropore volume decrease.

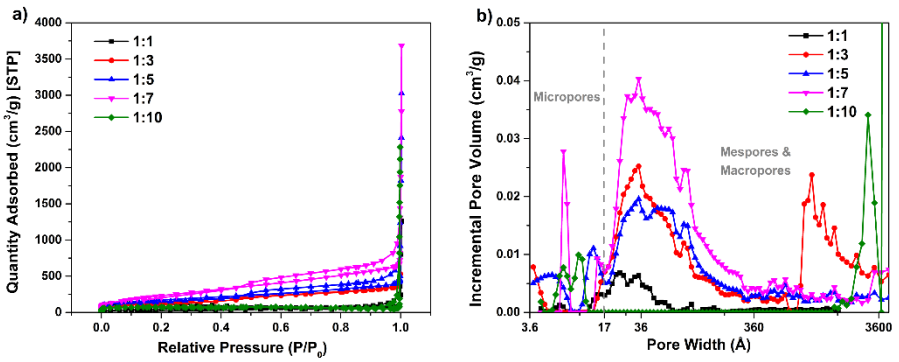

Figure 4-5. N_2 adsorption data for porous rGO at different GO:KOH ratio. (a) Isotherms obtained for samples. (b) Pore size distribution for each sample.

Table 4-1. BET specific surface area and porosity data of all rGO samples.

Sample	BET area (m^2g^{-1})	Micropore volume (<17Å) (cm^3g^{-1})	Meso & macro pore volume (17<V<3500Å) (cm^3g^{-1})
1:1	174	0.02	0.08
1:3	528	0.03	0.49
1:5	625	0.10	0.48
1:7	393	0.09	0.88
1:10	255	0.06	0

4.3. THERMAL ANALYSIS

The thermal behavior of KOH-treated GO samples are studied by differential scanning calorimetry (DSC) in the temperature range from room temperature to 1000 ℃. The DSC isotherms for the samples with GO:KOH ratio 1:0.5, 1:1 and 1:7 are shown in Figure 4-6. In Figure 4-6(a), the isotherm of the 1:0.5 sample shows an exothermal peak in the range of 100 ~ 210 ℃. As we discussed in Section 3.1, this peak arises from the reduction of functional groups. Between 700 and 950 ℃, two endothermic peaks could be seen, corresponding to the activation reactions which occur above 700℃ and the melting of the by-products K_2CO_3 around 891 ℃ [104,105]. In Figure 4-6(b), with increasing amount of KOH, between 100 and 210 ℃, an endothermal signal shows up, while the area of the exothermal peak decreases. Between 700 and 950 ℃, only the K_2CO_3 melting peak exists and the signal of the activation process could not be observed. We infer that the peak corresponding to the activation reactions is obscured by the large K_2CO_3 melting curve. The isotherm of the 1:7 sample shows only an endothermic peak (Figure 4-6(c)). Normally, GO can undergo deoxygenation in strongly alkaline conditions at room temperature [59,106,107]. With this effect, when large quantity of KOH is added into GO, most functional groups of GO are already decomposed at room temperature, leading to only the endothermal peak is left, which corresponds the water evaporation.

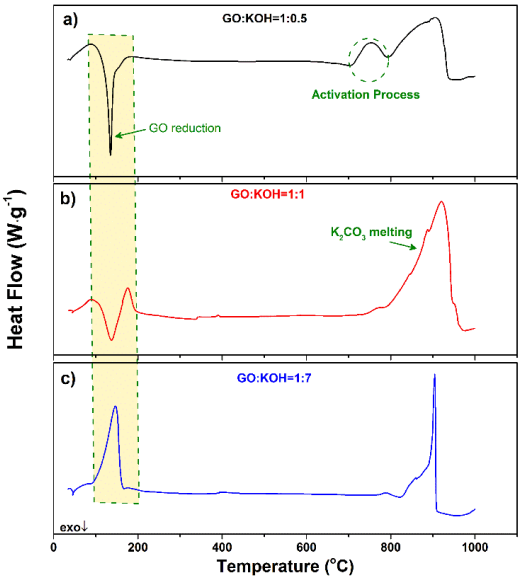

Figure 4-6. DSC isotherms for KOH-treated GO samples at different GO:KOH ratios: (a) 1:0.5. (b) 1:1. (c) 1:7.

The activation of GO by KOH normally starts to occur at around 700 ℃ (as shown in Figure 4-6). To explore the activation energy of this reaction, isothermal gravimetric analysis is carried out for the 1:3 sample at six different temperatures (600, 620, 640, 660, 680 and 700 ℃) for 4 h in argon atmosphere. In Figure 4-7(a), the curves show the relationship between time t and relative mass loss ρ. It is necessary to note that, the GO has been reduced before reaching the temperatures of interest, most functional groups have been removed, and the reaction of the GO carbon basal planes with KOH would be the only one occurring. As carbon is stable in inert gases below 1000 ℃, the contribution from the thermal degradation of the carbon backbone to ρ could be assumed to be negligibly small. At 600 ℃, the relative mass loss is around 1.44%. With an increase in temperature, ρ progressively rises to 4.2%. Higher temperature assists the GO-KOH reaction. In Figure 4-7(b), the relative activation energy E_a is calculated by the MacCallum method [62,63], the equation is described in Section 3.2. The value of E_a is found to be nearly constant, 179 ± 2 kJ/mol.

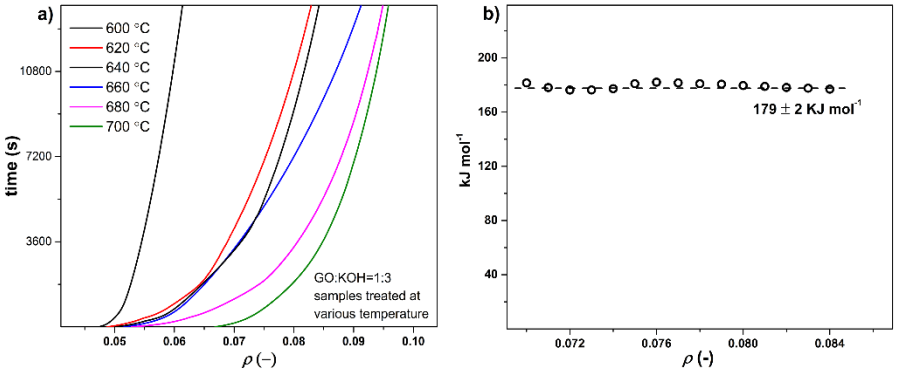

Figure 4-7. Isothermal Gravimetric Analysis of GO:KOH=1:3 sample. (a) The isothermal TG curves. (b) The calculated activation energy.

4.4. NANOPOROUS MEMBRANE FABRICATION

After investigating the activation process dynamics and the effects of different ratio of KOH on the morphology of the activated rGO, we apply this porous rGO material into membrane fabrication.

The fabricated porous rGO membrane through drop-casting are shown in Figure 4-8. The original GO membrane, which is made from 3 g/L GO solution directly, is quite flexible and shows a smooth and shiny surface. After annealing at 700 ℃ for 1 h, the produced rGO membrane becomes fragile. Besides, it is observed that many bubbles and wrinkles are found on its surface, which may be owing to the release of gases such as H_2O, CO_2 and CO during annealing.

However, after the addition of KOH, we could not fabricate a large size and integrated membrane successfully. In Figure 4-8, it could be seen that on a 1×1 cm^2 SiC substrate, the membrane is always not contiguous and fragmented. Fabrication was attempted with different concentrations of the solution (3, 5 and 10 g/L) for different ratios of GO:KOH (1:1, 1:3, 1:5, 1:7 and 1:10). With low concentration of the solution, for example 1:3 (3 g/L) sample, most of GO sheets are decomposed during activation process. With high concentration, e.g. 1:3 (10 g/L), the final membrane would undergo considerable shrinkage and delamination from the substrate. Upon increasing the ratio of KOH, the membranes are still fragmented, as shown in 1:5 samples. For 1:7 and 1:10 samples, only black fragments are observed on the substrate.

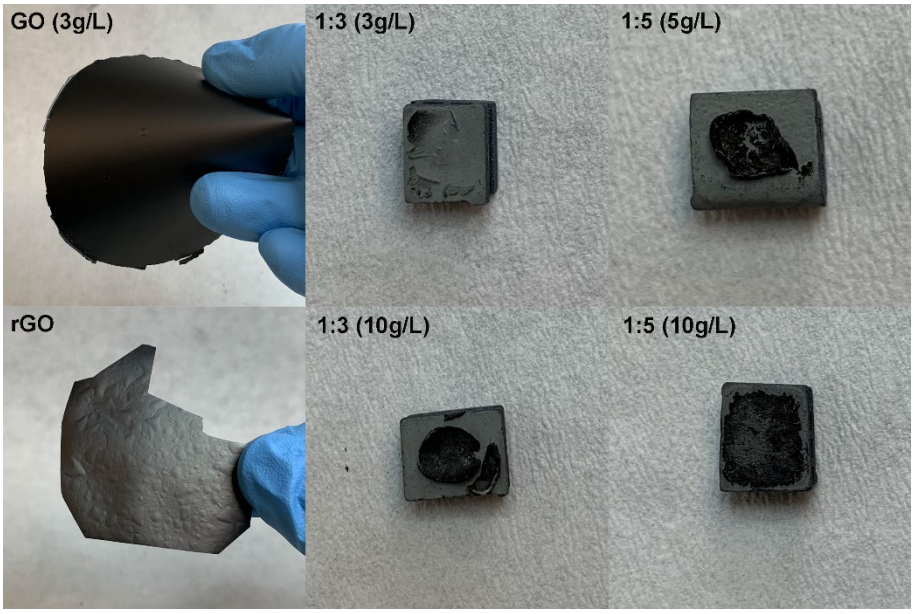

Figure 4-8. Images of GO and prepared rGO membranes.

The samples shown in Figure 4-8 are further analyzed by SEM in order to study their morphology. The corresponding micrographs are shown in Figure 4-9. In the 1:1 sample, there are many deposits areas on the membrane surface. With increasing of amount of KOH, these deposits aggregate and form the crystalline. Energy Dispersive X-ray Detector (EDX) data (Figure 4-10 and Table 4-2) shows that these deposits are mainly potassium salts. In 1:3 sample, the white spots cover the entire surface of the rGO membrane. In 1:5 and 1:7 samples, neither an rGO membrane nor the potassium salt deposits are observed. As discussed above, high ratios of KOH causes serious damage to the rGO sheets. The fragmentary rGO does not form continues layers and undergoes delamination from the substrate.

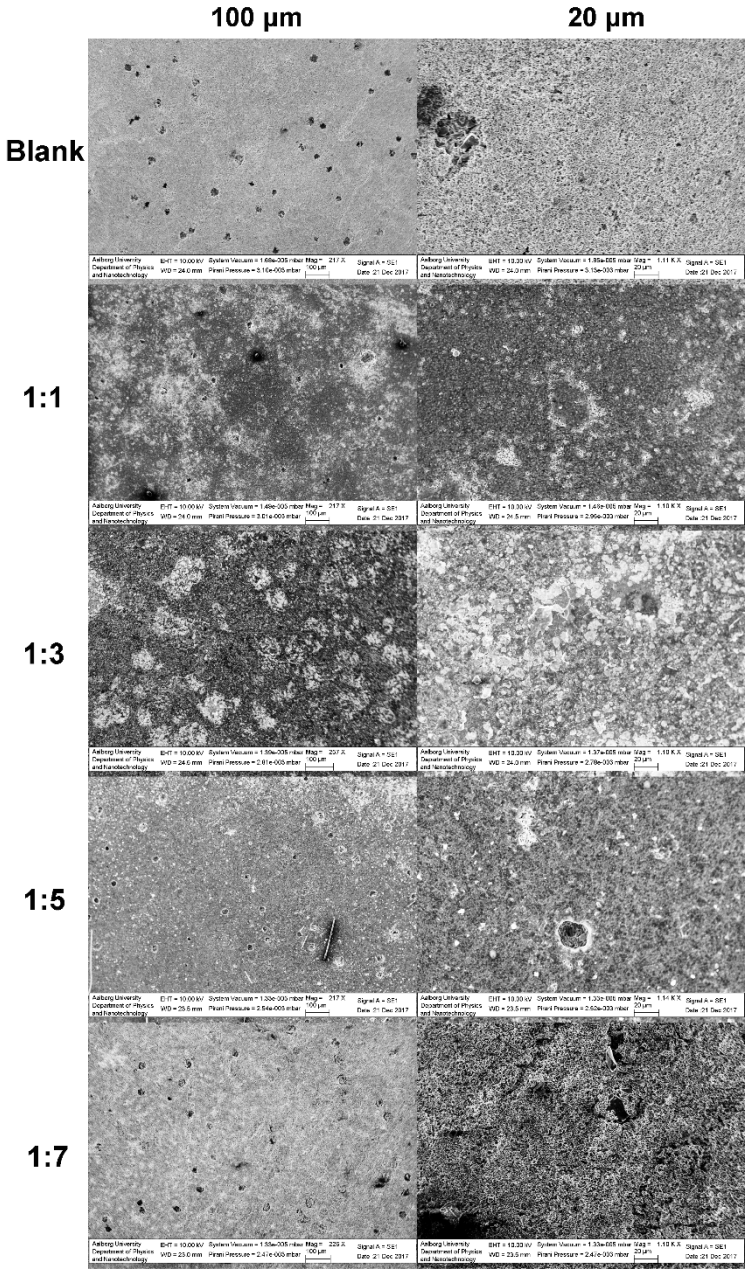

Figure 4-9. SEM images of the porous rGO membrane.

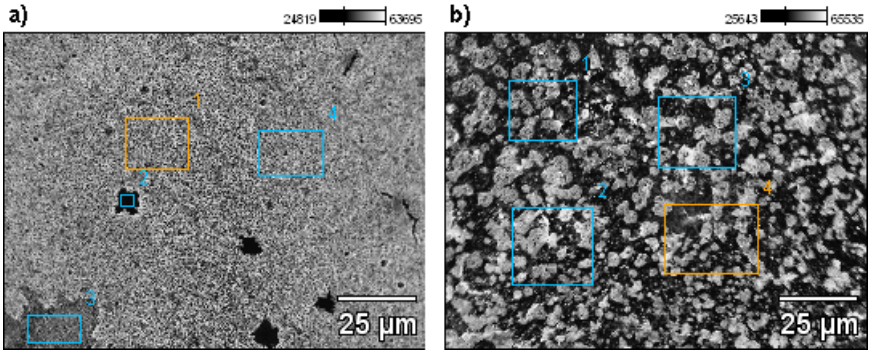

Figure 4-10. EDX scan of substrate and 1:3 sample.

Table 4-2. EDX data of substrate and 1:3 sample, the unit is weight%.

Sample NO.	C	O	Si	K
Substrate	33.89	8.72	57.16	__
1:3	58.65	16.33	14.48	6.69

4.5. SUMMARY

In this Chapter, porous rGO materials obtained by high-temperature activation of GO by KOH are explored for fabrication of membrane. The fabrication of both free-standing membranes as well as supported membranes on SiC substrate is attempted. With proper ratio of GO:KOH, it is possible to obtain activated rGO with a large surface area and pores on the carbon basal plane. However, when large amounts of KOH are added, the graphene sheets disintegrate, resulting in powdery rGO materials, which undergo delamination from the substrate. Although such supported rGO membranes would have considerable potential for water filtration, their fabrication remains a major challenge and is needed to be further explored.

CHAPTER 5. POROUS REDUCED GRAPHENE OXIDE-POLYMER FOR MEMBRANE

Polymer based nanoporous membranes are key components in water purification technologies, as they are low cost and could be easily synthetized and processed[108–110]. However, polymer membranes are generally accompanied by mechanical and chemical stability problems[111].

Graphene oxide based membranes, a rising star with 2D molecular configuration, have attracted huge attention owing to their remarkable water permeation characteristics. However, GO membranes are usually not very chemically and thermally stable. Besides, although the reduced GO (rGO) has highly stability, its connectivity is poor.

In this experiment, we produced nanocomposites of the polymer allylhydridopolycarbosilane (AHPCS) with rGO for membrane application. The polymer acts as binder for holding rGO platelets together after pyrolysis [112]. Continuous membranes of the nanocomposite incorporating the rGO could be obtained.

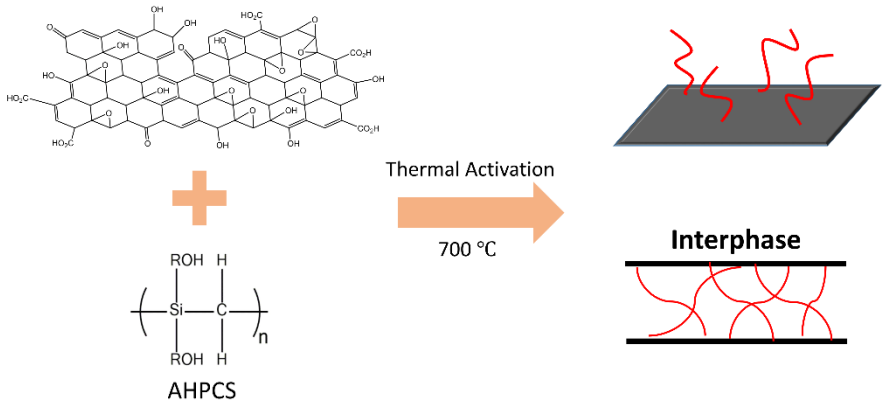

Schematic 5-1. Fabrication of reduced Graphene Oxide composite materials.

5.1. CHARACTERIZATION OF GO-POLYMER COMPOSITE

Different mass ratio of raw GO samples and AHPCS are mixed in Tetrahydrofuran (THF): GO:AHPCS = 1:0.5, 1:1, 1:10 and 1:100. The concentration of GO is 0.1 and 0.3 weight%. After annealed at 700 ℃ for 1h in Ar atmosphere, the obtained samples are analyzed by FTIR and XRD, as shown in Figure 5-1.

Figure 5-1(a) shows the FTIR spectra of GO, rGO and 100-0.1% (GO:AHPCS = 1:100, GO concentration is 0.1%) samples. The structures of GO and rGO have been discussed in Chapter 3. There are four species of functional groups in GO: hydroxyl, epoxide, carbonyl and carboxyl. After thermal reduction, only C-OH, C=C and epoxides are left in rGO. However, when GO is mixed with AHPCS and annealed under the same condition, there is no related oxygen signal could be observed in FTIR profile. Only Si-C bond, which is located at 1084 cm^{-1} [113–115], shows up. We infer that the polymeric AHPCS molecules are fully covered the carbon sheets so that the FTIR curve of this composite shows a broad Si-C bond peak.

Figure 5-1(b) presents the XRD patterns for three samples: original GO, rGO and 100-0.1% composite. GO shows a sharp peak at around 11^o, which corresponds to an interlayer distance of around 0.7 nm, while rGO has a broad peak at around 25^o, corresponding to an interlayer spacing of around 0.36 nm. However, no peak is observed in case of the 100-0.1% sample implying that the concentration of rGO is very low.

The other GO+AHPCS composite samples depict the same FTIR and XRD profiles. We infer that the polymeric AHPCS molecules fully insert into GO interlayers and bond to the carbon network. After annealing, the GO sheets are strongly bonded to the polysilicon carbide molecules. Besides, the AHPCS materials completely envelop the graphene sheets, as a result of which the characteristic XRD peaks of GO could not be detected.

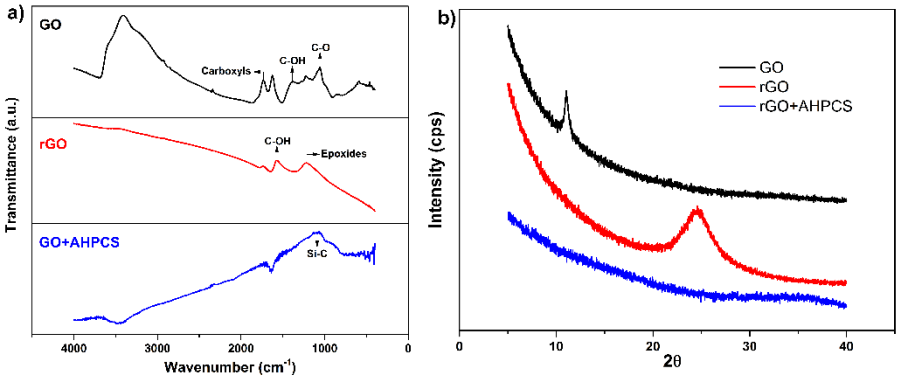

Figure 5-1. FTIR and XRD data of GO, rGO and prepared 1:100 (0.1%) composites.

Figure 5-2 shows the N_2 adsorption analysis of the 100-0.1% sample. Figure 5-2(a) is the cumulative pore volume curve. Based on the BET method, the specific surface area of this sample is 49.01 m^2/g. This is significantly lower than the specific surface area of 625 m^2/g observed for the KOH-treated porous rGO materials. It could be deduced that, although the AHPCS polymer bring acts as an effective binder for the GO sheet, the polymer molecules also block the defects and disorders in the GO, resulting in a decrease in the specific surface of the composite.

Figure 5-2(b) shows the pore size distribution of 100-0.1% sample. For this composite material, no micropore (< 30 Å) could be detected. This is probably owing to the fact that the small defects are easily covered by the AHPCS molecules. The pore width is mainly distributed in the range of 30~100 Å, which lies in the mesoporous range. The volume of the mesopores is around 0.04 cm^3g^{-1}. No macropores above 1000 Å could be observed, unlike in the case of activated rGO membranes described in Chapter 4. The total area in pores in the range of 20 and 2500 Å, is around 14.05 m^2g^{-1}.

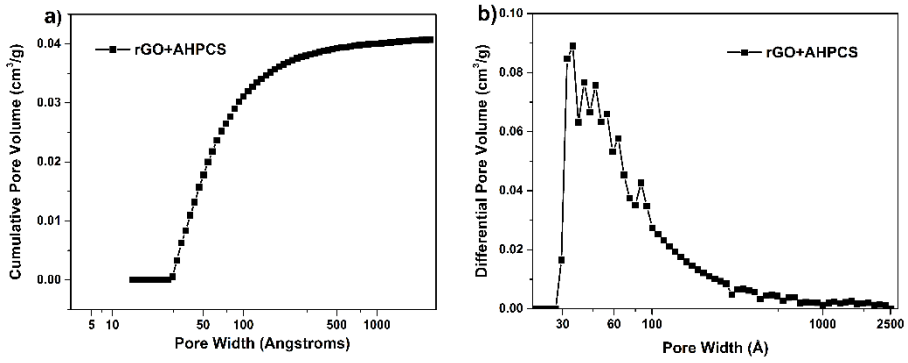

Figure 5-2. N_2 adsorption data for nanocomposite rGO sample.

5.2. NANOCOMPOSITE MEMBRANE FABRICATION

GO+AHPCS membranes are fabricated by drop-casting solutions containing different ratios of GO:AHPCS on SiC substrate, followed by annealing at 700 ℃ for 1 h. The produced membranes are shown in Figure 5-3. For blank reference sample, it shows a dark grey color. After been covered with pure AHPCS polymer, the color of substrate does not change much and is still dark grey, which implies that the color's changing of the following samples does not depends on the concentration of AHPCS much. The GO membrane without annealing shows a dark brown color. For the 100-0.1% sample, the membrane appears similar to the GO membrane, but has a corrugated surface. Nevertheless, the composite membrane is continuous and has integrity. With increasing amount of GO, from GO:AHPCS ratios of 1:100 to 1:1, the color of membrane becomes progressively lighter. The 1-0.1% sample appears shining grey, but is a continuous film. However, when the mass ratio of GO:AHPCS decreases to 1:0.5 (0.1%), a continuous membrane could not be obtained. Also, the GO distribution in the polymer is uneven, and aggregates are visible to the eye.

In addition to the effect of mass ratio of GO and AHPCS on the membrane formation, the concentration of GO in the solution used to prepare the membranes is studied as well. For GO:AHPCS ratios of 1:100 and 1:1, 0.3 weight% GO is used during the fabrication, as shown in the last two images in Figure 5-3. For the 100-0.3% sample, a very dark the membrane is obtained. When the ratio GO:AHPCS decreases to 1:1 (0.3%), the composite does not form a continuous membrane. The center area breaks into pieces. We deduce that when excessive amount of GO is added, the color of the composite more depends on the graphene layers after annealed; besides, the limited content of AHPCS could not bind such many GO carbon resulting in the membrane is broken at low ratio of AHPCS.

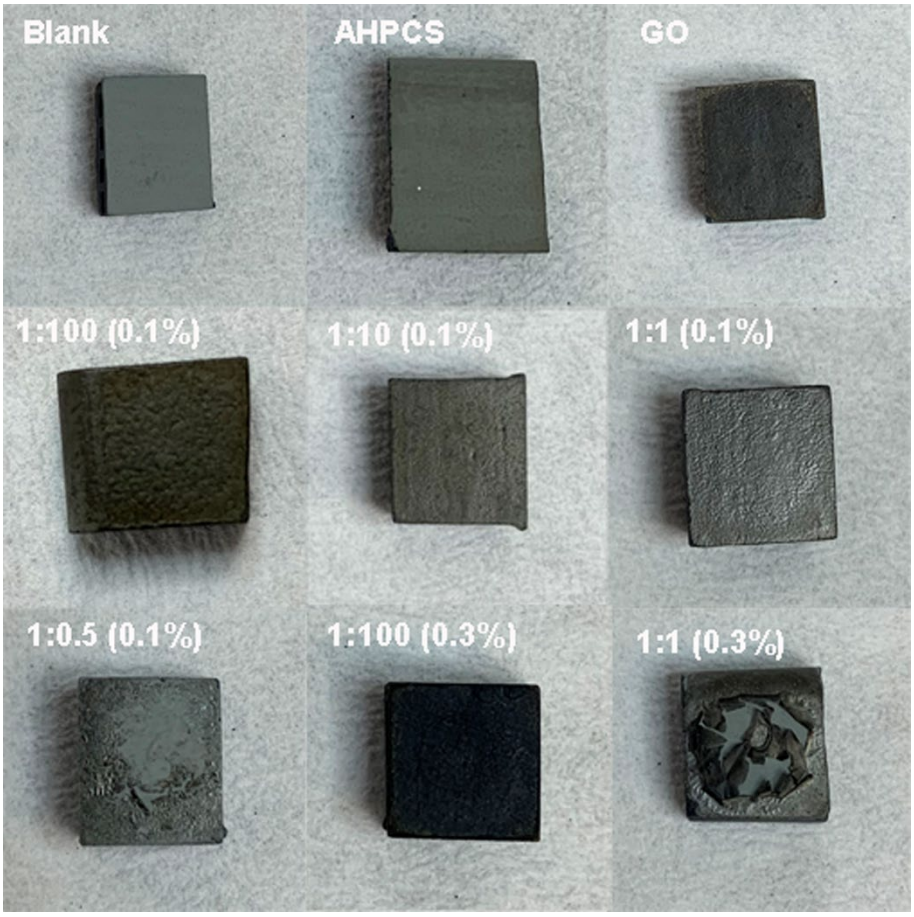

Figure 5-3. Images of different ratio of GO+AHPCS membranes.

The effect of surface roughness and surface energy on the wettability of the different ratio GO:AHPCS membranes are measured by the static contact angle with water, the images are shown in Figure 5-4. For the original GO membrane, the contact angle is around 53.8°. GO membrane is hydrophilic because of the existence of oxygen-containing functional groups on the graphene. After the addition of polymer AHPCS and annealing, the contact angle increases to 64.56° for 100-0.1% sample. With a decrease of AHPCS mass ratio, the contact angle of the membrane decreases. Moreover, for the same ratio of GO:AHPCS=1:100, increase in the concentration of GO from 1% to 3% results in an increase in contact angle of the produced membrane from 64.56° to 69.21°. This may be owing to the fact that, at higher concentration, the graphene layers are not sufficiently exfoliated in the starting solution, and hence, not well-enclosed in the polymer in the membrane. Graphene pellet have been reported to have a contact angle of 89.8°, and graphite, 115° [116–118]. By comparison, the

contact angle of the GO+AHPCS composite is much smaller, which may be owing the hydrophilic nature of AHPCS.

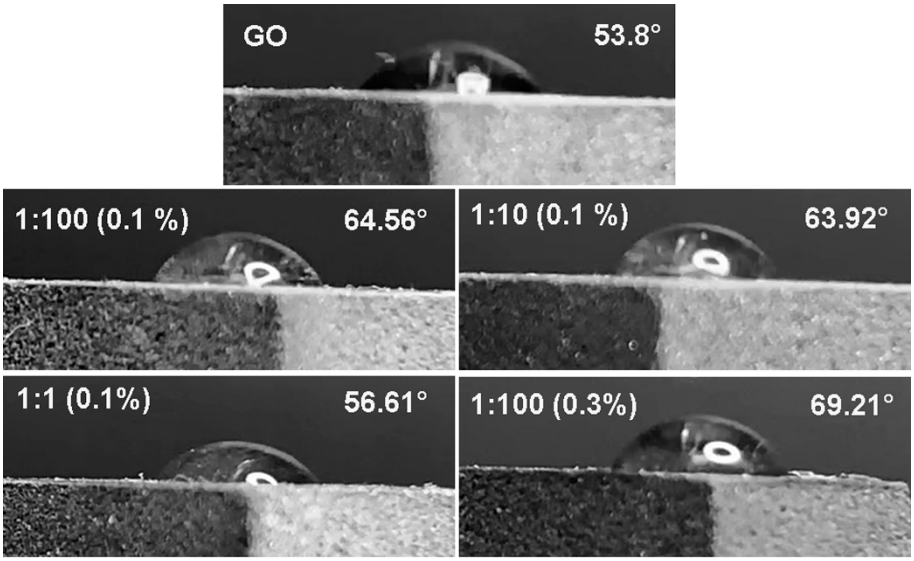

Figure 5-4. Images of contact angle of different ratio of GO+AHPCS membranes.

As the membranes are fabricated through annealing at 700 ℃ in Ar atmosphere, it indicates that this composite membrane has highly thermal resistance under inert condition. The heat stability in air of the GO+AHPCS membranes are also investigated. Three samples are selected at the ratios of GO:AHPCS=1:100, 1:10 and 1:1, the concentration of GO is 0.1%. The membrane samples are thermal treated at 200 and 300 ℃ in air for 30 min, the results are shown in Figure 5-5. At room temperature, the three samples present a continuous dark membranes. After annealing at 200 ℃ in air, all of these membranes do not change much and retain the integrity. To our surprise, even after 300 ℃ annealing in air, the membranes are still stacked on the substrates tightly and no broken area could be seen. This outstanding thermal resistance has beyond most polymeric composite membranes.

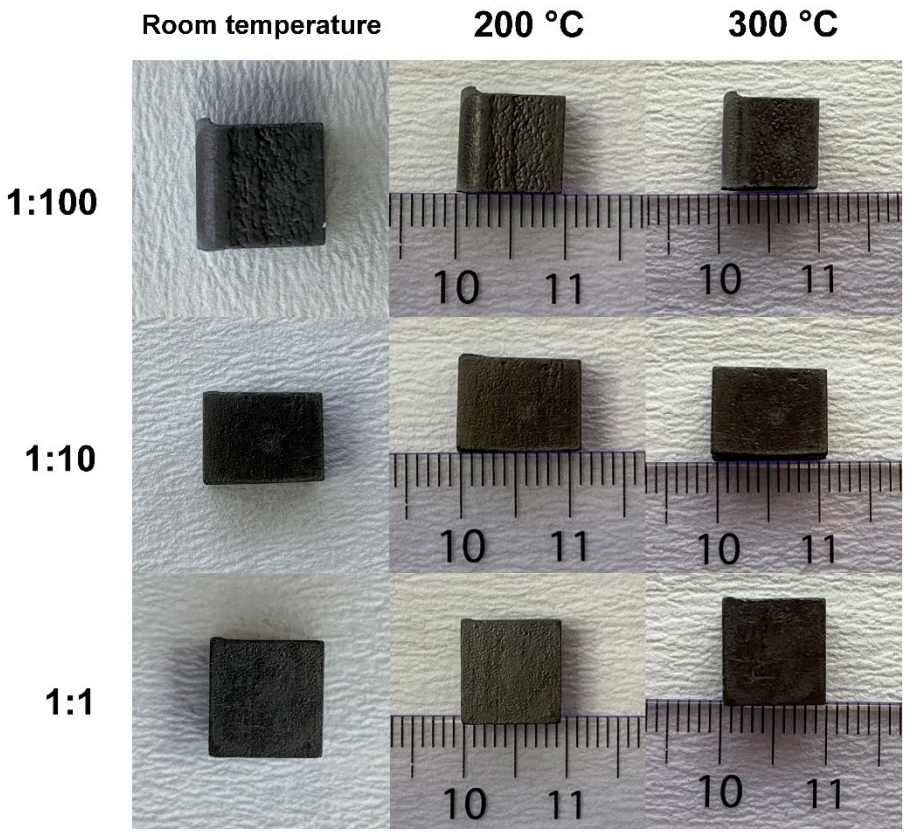

Figure 5-5. Images of different ratio of GO+AHPCS membranes (0.1%) after annealed at various temperature in air for 30 min.

5.3. SUMMARY

In this Chapter, GO+AHPCS nanocomposites are explored for membrane fabrication through drop-casting. The use of AHPCS as a binder enables the production of continuous membrane films, which is not possible for KOH-activated porous GO, as described in Chapter 4. AHPCS material is not only an effective matrix for incorporating GO but could also withstand a high annealing temperature of 700 ℃. The GO+AHPCS nanocomposite membranes are characterized by FTIR and XRD. As the polymer molecules fully covered the graphene sheets and the pores therein, the composites do not have large specific surfaces. The nanocomposites are found suitable for the fabrication of continuous and integrated membranes, which are found by contact angle measurements to be hydrophilic property and also ultra-thermally stable. This GO+AHPCS composite has great potential for membrane researches.

CHAPTER 6. CONCLUSIONS AND PERSPECTIVE

6.1. CONCLUSIONS

In this thesis, which focuses on the structural evolution and potentials applications of graphene oxide (GO), the following three research subjects are investigated: (1) the mechanisms of low-temperature GO reduction (Chapter 3); (2) pore-formation in reduced GO (rGO) for membrane fabrication (Chapter 4); (3) highly stable SiC-rGO nanocomposites for separation technique (Chapter 5). The findings in these subjects are here summarized.

GO is a low-cost precursor of graphene as it can be easily converted into graphene-like materials by thermal reduction. Therefore, developing a deep knowledge of the mechanisms involved in the reduction process is vital. We provide insight into the chemical evolution, structural transition and thermal dynamics of GO reduction between 100 and 300 ℃. Our results demonstrate that the reduction process can be divided into 3 distinct steps: Step 1 (below 160 ℃), which consists in the evaporation of physical adsorbed water; Step 2 (between 160 and 210 ℃) resulting from the decomposition of liable functional groups; Step 3 (between 210 and 300 ℃) which corresponds to the degradation of the most stable functionalities and of the sulfates impurities, which are commonly present in Hummers' GO. Different from previous studies, we discovered that GO thermal reduction process is not a single exothermic reaction. On the contrary, Step 3 involves independent endothermic reactions. The activation energy of Step 2 is nearly constant, E_a = 112 ± 6 kJ/mol, while Step 3's activation energy increases gradually and reaches 248 ± 9 kJ/mol. GC-MS data show that the by-products of Step 2 are mainly CO_2, CO and H_2O; for Step 3, also SO_2 and some aromatic volatile compounds are detected. About the chemical evolution of GO, FTIR and XPS measurements show that C-OH and C-O groups are removed easily, but a large number of epoxy, carboxyl and S-O bonds could not be decomposed below 200 ℃. Raman spectroscopy and XRD indicate that, as a result of the degradation of GO functional groups, large areas in the GO planes are concerted to disordered and defective structures and the interlayer spacing of carbon sheets decreases from 0.694 nm to 0.362 nm.

For nanoporous reduced GO material, we explore the usability of KOH activated porous GO for membrane fabrication. Through XRD, we know that the main products of the reaction between GO and KOH at 700 ℃ are K_2CO_3 and K_2O. After removing these by-products, the porous GO has a similar XRD profile as normal rGO samples, i.e. shows a broad peak located at 2θ of about 25°. The isothermal TG data confirm that the activation energy of this process is 179 ± 2 kJ/mol. The N_2 adsorption results

show that the BET surface area could reach 625 m^2g^{-1} when the mass ratio of GO:KOH = 1:5, but excessive addition of KOH would decrease the BET area. Based on morphology observation, higher amount of KOH leads to powdery samples. Under these conditions, GO carbon sheets are seriously damaged and a large quantity of defects is generated at the detriment of the structural stability of the material.

Concerning SiC-rGO nanocomposite materials for water separation technologies, a special polymer allylhydridopolycarbosilane (AHPCS), which could be converted to SiC at 700 ℃, is chosen. The FTIR spectra of the produced rGO nanocomposite present no peaks of oxygen functional groups and the XRD analysis revealed the sample to be amorphous. N_2 adsorption porosimetry shows that the material to be porous with a size distribution ranging from 30 to 2500 Å and a BET surface area surface area of 49.01 m^2g^{-1}. With proper ratio of GO and AHPCS, this nanocomposite could form a continuous membrane with a good adhesion on a porous SiC substrate with hydrophilic properties (contact angle = $50^o \sim 69^o$). Moreover, this nanocomposite membrane has high thermal resistance, since it can keep its integrity after annealing in air at 300 ℃ for 30 min.

6.2. PERSPECTIVE

With regard to the GO thermal reduction process, different reaction steps during annealing should be taken into consideration in designing and manufacturing industrial scale graphene-like products. Particularly, impurities, as sulfates, have a non-negligible effect on the thermal response of the material reduction.

The related reduced GO materials have better chemical and thermal stability compared to the original GO. Therefore, they are suitable for the fabrication of new type membranes. Generating porous structure in rGO is desirable for high water permeability. But how to coat the membrane material on large-area porous substrates still deserve to be explored. The addition of polymer, as ceramic precursors, could be an effective method. In our study, AHPCS allows to fabricate continuous layers with great integrity. Nevertheless, the ability of the resulting SiC-rGO composite layer to act as a membrane for water purification still need to be investigated.

CHAPTER 7. BIBLIOGRAPHY

[1] J. Lubchenco, Entering the century of the environment: A new social contract for science, Science. 279 (1998) 491–497.

[2] F. Perreault, A. Fonseca De Faria, M. Elimelech, Environmental applications of graphene-based nanomaterials, Chem. Soc. Rev. 44 (2015) 5861–5896.

[3] K.S. Novoselov, A. Mishchenko, A. Carvalho, A.H. Castro Neto, 2D materials and van der Waals heterostructures, Science. 353 (2016) aac9439.

[4] M.G. Stanford, P.D. Rack, D. Jariwala, Emerging nanofabrication and quantum confinement techniques for 2D materials beyond graphene, Npj 2D Mater. Appl. 2 (2018) 20.

[5] M. Akhtar, G. Anderson, R. Zhao, A. Alruqi, J.E. Mroczkowska, G. Sumanasekera, J.B. Jasinski, Recent advances in synthesis, properties, and applications of phosphorene, Npj 2D Mater. Appl. 1 (2017) 5.

[6] M. Xu, T. Liang, M. Shi, H. Chen, Graphene-like two-dimensional materials, Chem. Rev. 113 (2013) 3766–3798.

[7] S.Z. Butler, S.M. Hollen, L. Cao, Y. Cui, J.A. Gupta, H.R. Gutiérrez, T.F. Heinz, S.S. Hong, J. Huang, A.F. Ismach, E. Johnston-Halperin, M. Kuno, V. V. Plashnitsa, R.D. Robinson, R.S. Ruoff, S. Salahuddin, J. Shan, L. Shi, M.G. Spencer, M. Terrones, W. Windl, J.E. Goldberger, Progress, challenges, and opportunities in two-dimensional materials beyond graphene, ACS Nano. 7 (2013) 2898–2926.

[8] N. Drnovšek, The translation of the seat of metropolitanate of Kiev from Kiev to Moscow, Bogosl. Vestn. 78 (2018) 135–146.

[9] A.K. Geim, K.S. Novoselov, The rise of graphene, Nat. Mater. 6 (2007) 183–191.

[10] G. Eda, M. Chhowalla, Chemically derived graphene oxide: Towards large-area thin-film electronics and optoelectronics, Adv. Mater. 22 (2010) 2392–2415.

[11] S. Hu, M. Lozada-Hidalgo, F.C. Wang, A. Mishchenko, F. Schedin, R.R. Nair, E.W. Hill, D.W. Boukhvalov, M.I. Katsnelson, R.A.W. Dryfe, I. V. Grigorieva, H.A. Wu, A.K. Geim, Proton transport through one-atom-thick crystals, Nature. 516 (2014) 227–230.

[12] J.S. Bunch, S.S. Verbridge, J.S. Alden, A.M. Van Der Zande, J.M. Parpia, H.G. Craighead, P.L. McEuen, Impermeable atomic membranes from graphene sheets, Nano Lett. 8 (2008) 2458–2462.

[13] Y. Su, V.G. Kravets, S.L. Wong, J. Waters, A.K. Geim, R.R. Nair, Impermeable barrier films and protective coatings based on reduced graphene oxide, Nat. Commun. 5 (2014) 1–5.

[14] C. Lee, X. Wei, J.W. Kysar, J. Hone, Measurement of the elastic properties and intrinsic strength of monolayer graphene, Science. 321 (2008) 385–388.

[15] A.C. Ferrari, F. Bonaccorso, V. Fal'ko, K.S. Novoselov, S. Roche, P. Bøggild, S. Borini, F.H.L. Koppens, V. Palermo, N. Pugno, J.A. Garrido, R. Sordan, A. Bianco, L. Ballerini, M. Prato, E. Lidorikis, J. Kivioja, C. Marinelli, T. Ryhänen, A. Morpurgo, J.N. Coleman, V. Nicolosi, L. Colombo, A. Fert, M. Garcia-Hernandez, A. Bachtold, G.F. Schneider, F. Guinea, C. Dekker, M. Barbone, Z. Sun, C. Galiotis, A.N. Grigorenko, G. Konstantatos, A. Kis, M. Katsnelson, L. Vandersypen, A. Loiseau, V. Morandi, D. Neumaier, E. Treossi, V. Pellegrini, M. Polini, A. Tredicucci, G.M. Williams, B. Hee Hong, J.H. Ahn, J. Min Kim, H. Zirath, B.J. Van Wees, H. Van Der Zant, L. Occhipinti, A. Di Matteo, I.A. Kinloch, T. Seyller, E. Quesnel, X. Feng, K. Teo, N. Rupesinghe, P. Hakonen, S.R.T. Neil, Q. Tannock, T. Löfwander, J. Kinaret, Science and technology roadmap for graphene, related two-dimensional crystals, and hybrid systems, Nanoscale. 7 (2015) 4598–4810.

[16] M.D. Stoller, S. Park, Y. Zhu, J. An, R.S. Ruoff, Graphene-Based Ultracapacitors, Nano Lett. 8 (2008) 3498–3502.

[17] J. Liu, L. Cui, D. Losic, Graphene and graphene oxide as new nanocarriers for drug delivery applications, Acta Biomater. 9 (2013) 9243–9257.

[18] X. Li, X. Wang, L. Zhang, S. Lee, H. Dai, Chemically derived, ultrasmooth graphene nanoribbon semiconductors., Science. 319 (2008) 1229–32.

[19] L. Chen, G. Shi, J. Shen, B. Peng, B. Zhang, Y. Wang, F. Bian, J. Wang, D. Li, Z. Qian, G. Xu, G. Liu, J. Zeng, L. Zhang, Y. Yang, G. Zhou, M. Wu, W. Jin, J. Li, H. Fang, Ion sieving in graphene oxide membranes via cationic control of interlayer spacing, Nature. 550 (2017) 1–4.

[20] D.R. Dreyer, S. Park, C.W. Bielawski, R.S. Ruoff, The chemistry of graphene oxide, Chem. Soc. Rev. 39 (2010) 228–240.

[21] D.A. Dikin, S. Stankovich, E.J. Zimney, R.D. Piner, G.H.B. Dommett, G. Evmenenko, S.T. Nguyen, R.S. Ruoff, Preparation and characterization of

graphene oxide paper, Nature. 448 (2007) 457–460.

[22] L. Staudenmaier, Verfahren zur Darstellung der Graphits??ure, Berichte Der Dtsch. Chem. Gesellschaft. 32 (1899) 1394–1399.

[23] W.S. Hummers, R.E. Offeman, Preparation of Graphitic Oxide, J. Am. Chem. Soc. 80 (1958) 1339.

[24] B.C. Brodie, On the Atomic Weight of Graphite, Philos. Trans. R. Soc. London. 149 (1859) 249–259.

[25] S. Pei, H.M. Cheng, The reduction of graphene oxide, Carbon. 50 (2012) 3210–3228.

[26] O.C. Compton, S.T. Nguyen, Graphene oxide, highly reduced graphene oxide, and graphene: Versatile building blocks for carbon-based materials, Small. 6 (2010) 711–723.

[27] Y. Zhu, S. Murali, W. Cai, X. Li, J.W. Suk, J.R. Potts, R.S. Ruoff, Graphene and graphene oxide: Synthesis, properties, and applications, Adv. Mater. 22 (2010) 3906–3924.

[28] X. Huang, Z. Yin, S. Wu, X. Qi, Q. He, Q. Zhang, Q. Yan, F. Boey, H. Zhang, Graphene-based materials: Synthesis, characterization, properties, and applications, Small. 7 (2011) 1876–1902.

[29] S. Guo, S. Dong, Graphene nanosheet: Synthesis, molecular engineering, thin film, hybrids, and energy and analytical applications, Chem. Soc. Rev. 40 (2011) 2644–2672.

[30] C. Zhang, W. Lv, X. Xie, D. Tang, C. Liu, Q.H. Yang, Towards low temperature thermal exfoliation of graphite oxide for graphene production, Carbon. 62 (2013) 11–24.

[31] W. Lv, D.M. Tang, Y.B. He, C.H. You, Z.Q. Shi, X.C. Chen, C.M. Chen, P.X. Hou, C. Liu, Q.H. Yang, Low-temperature exfoliated graphenes: Vacuum-promoted exfoliation and electrochemical energy storage, ACS Nano. 3 (2009) 3730–3736.

[32] A. Kaniyoor, T.T. Baby, S. Ramaprabhu, Graphene synthesis via hydrogen induced low temperature exfoliation of graphite oxide, J. Mater. Chem. 20 (2010) 8467–8469.

[33] B. Shen, D. Lu, W. Zhai, W. Zheng, Synthesis of graphene by low-

temperature exfoliation and reduction of graphite oxide under ambient atmosphere, J. Mater. Chem. C. 1 (2013) 50–53.

[34] L.L. Zhang, X. Zhao, M.D. Stoller, Y. Zhu, H. Ji, S. Murali, Y. Wu, S. Perales, B. Clevenger, R.S. Ruoff, Highly Conductive and Porous Activated Reduced Graphene Oxide Films for High-Power Supercapacitors, Nano Lett. 12 (2012) 1806–1812.

[35] F. Perreault, A. Fonseca De Faria, M. Elimelech, Environmental applications of graphene-based nanomaterials, Chem. Soc. Rev. 44 (2015) 5861–5896.

[36] T.S. Sreeprasad, V. Berry, How do the electrical properties of graphene change with its functionalization?, Small. 9 (2013) 341–350.

[37] S. Park, R.S. Ruoff, Chemical methods for the production of graphenes, Nat. Nanotechnol. 4 (2009) 217–224.

[38] C. Hontoria-Lucas, A.J. López-Peinado, J. de D. López-González, M.L. Rojas-Cervantes, R.M. Martín-Aranda, Study of oxygen-containing groups in a series of graphite oxides: Physical and chemical characterization, Carbon. 33 (1995) 1585–1592.

[39] G. Liu, W. Jin, N. Xu, Two-Dimensional-Material Membranes: A New Family of High-Performance Separation Membranes, Angew. Chemie - Int. Ed. 55 (2016) 13384–13397.

[40] G. Liu, W. Jin, N. Xu, Graphene-based membranes, Chem. Soc. Rev. 44 (2015) 5016–5030.

[41] H. Huang, Y. Ying, X. Peng, Graphene oxide nanosheet: An emerging star material for novel separation membranes, J. Mater. Chem. A. 2 (2014) 13772–13782.

[42] K.A. Mahmoud, B. Mansoor, A. Mansour, M. Khraisheh, Functional graphene nanosheets: The next generation membranes for water desalination, Desalination. 356 (2015) 208–225.

[43] M. Deng, K. Kwac, M. Li, Y. Jung, H.G. Park, Stability, Molecular Sieving, and Ion Diffusion Selectivity of a Lamellar Membrane from Two-Dimensional Molybdenum Disulfide, Nano Lett. 17 (2017) 2342–2348.

[44] P.S. Goh, A.F. Ismail, Graphene-based nanomaterial: The state-of-the-art material for cutting edge desalination technology, Desalination. 356 (2015) 115–128.

[45] R.R. Nair, H.A. Wu, P.N. Jayaram, I. V. Grigorieva, A.K. Geim, Unimpeded permeation of water through helium-leak-tight graphene-based membranes, Science. 335 (2012) 442–444.

[46] R.K. Joshi, P. Carbone, F.C. Wang, V.G. Kravets, Y. Su, I. V. Grigorieva, H.A. Wu, A.K. Geim, R.R. Nair, Precise and ultrafast molecular sieving through graphene oxide membranes, Science. 343 (2014) 752–754.

[47] J. Abraham, K.S. Vasu, C.D. Williams, K. Gopinadhan, Y. Su, C.T. Cherian, J. Dix, E. Prestat, S.J. Haigh, I. V. Grigorieva, P. Carbone, A.K. Geim, R.R. Nair, Tunable sieving of ions using graphene oxide membranes, Nat. Nanotechnol. 12 (2017) 546–550.

[48] A. Esfandiar, B. Radha, F.C. Wang, Q. Yang, S. Hu, S. Garaj, R.R. Nair, A.K. Geim, K. Gopinadhan, Size effect in ion transport through angstrom-scale slits, Science. 358 (2017) 511–513.

[49] Q. Zhang, X. Qian, K.H. Thebo, H.M. Cheng, W. Ren, Controlling reduction degree of graphene oxide membranes for improved water permeance, Sci. Bull. 63 (2018) 788–794.

[50] J.Y. Chong, B. Wang, K. Li, Water transport through graphene oxide membranes: The roles of driving forces, Chem. Commun. 54 (2018) 2554–2557.

[51] S. Zheng, Q. Tu, J.J. Urban, S. Li, B. Mi, Swelling of Graphene Oxide Membranes in Aqueous Solution: Characterization of Interlayer Spacing and Insight into Water Transport Mechanisms, ACS Nano. 11 (2017) 6440–6450.

[52] C.-N. Yeh, K. Raidongia, J. Shao, Q.-H. Yang, J. Huang, On the origin of the stability of graphene oxide membranes in water, Nat. Chem. 7 (2015) 166–170.

[53] F. Pendolino, N. Armata, T. Masullo, A. Cuttitta, Temperature influence on the synthesis of pristine graphene oxide and graphite oxide, Mater. Chem. Phys. 164 (2015) 71–77.

[54] A. Ganguly, S. Sharma, P. Papakonstantinou, J. Hamilton, Probing the thermal deoxygenation of graphene oxide using high-resolution in situ X-ray-based spectroscopies, J. Phys. Chem. C. 115 (2011) 17009–17019.

[55] P. Paufler, Introductory Solid State Physics, Taylor & Francis, 1991.

[56] W. Zhang, Y. Li, S. Peng, Facile Synthesis of Graphene Sponge from

Graphene Oxide for Efficient Dye-Sensitized H_2 Evolution, ACS Appl. Mater. Interfaces. 8 (2016) 15187–15195.

[57] M.J. McAllister, J.L. Li, D.H. Adamson, H.C. Schniepp, A.A. Abdala, J. Liu, M. Herrera-Alonso, D.L. Milius, R. Car, R.K. Prud'homme, I.A. Aksay, Single sheet functionalized graphene by oxidation and thermal expansion of graphite, Chem. Mater. 19 (2007) 4396–4404.

[58] Y. Qiu, F. Collin, R.H. Hurt, I. Külaots, Thermochemistry and kinetics of graphite oxide exothermic decomposition for safety in large-scale storage and processing, Carbon. 96 (2016) 20–28.

[59] X. Fan, W. Peng, Y. Li, X. Li, S. Wang, G. Zhang, F. Zhang, Deoxygenation of exfoliated graphite oxide under alkaline conditions: a green route to graphene preparation, Adv. Mater. 20 (2008) 4490–4493.

[60] K. Hu, X. Xie, T. Szkopek, M. Cerruti, Understanding Hydrothermally Reduced Graphene Oxide Hydrogels: From Reaction Products to Hydrogel Properties, Chem. Mater. 28 (2016) 1756–1768.

[61] J.I. Parades, S. Villar-Rodil, A. Martínez-Alonso, J.M.D. Tascón, Graphene oxide dispersions in organic solvents, Langmuir. 24 (2008) 10560–10564.

[62] J.R. MacCallum, Thermogravimetric analysis of polymers for assessing thermal degradation, Thermochim. Acta. 96 (1985) 275–281.

[63] A. Babanalbandi, D.J.T. Hill, D.S. Hunter, L. Kettle, Thermal stability of poly(lactic acid) before and after γ-radiolysis, Polym. Int. 48 (1999) 980–984.

[64] O. Jankovský, M. Lojka, M. Nováček, J. Luxa, D. Sedmidubský, M. Pumera, J. Kosina, Z. Sofer, Reducing emission of carcinogenic by-products in the production of thermally reduced graphene oxide, Green Chem. 18 (2016) 6618–6629.

[65] J.M. Tour, Pristine Graphite Oxide, J. Am. Chem. Soc. 134 (2012) 2815–2822.

[66] K. Haubner, J. Murawski, P. Olk, L.M. Eng, C. Ziegler, B. Adolphi, E. Jaehne, The route to functional graphene oxide, ChemPhysChem. 11 (2010) 2131–2139.

[67] G. Wang, J. Yang, J. Park, X. Gou, B. Wang, H. Liu, J. Yao, Facile Synthesis and Characterization of Graphene Nanosheets, J. Phys. Chem. C. 112 (2008) 8192–8195.

[68] S. Eigler, C. Dotzer, F. Hof, W. Bauer, A. Hirsch, Sulfur species in graphene oxide, Chem. - A Eur. J. 19 (2013) 9490–9496.

[69] P. V. Kumar, N.M. Bardhan, S. Tongay, J. Wu, A.M. Belcher, J.C. Grossman, Scalable enhancement of graphene oxide properties by thermally driven phase transformation, Nat. Chem. 6 (2014) 151–158.

[70] S. Eigler, C. Dotzer, A. Hirsch, Visualization of defect densities in reduced graphene oxide, Carbon. 50 (2012) 3666–3673.

[71] W. Chen, L. Yan, P.R. Bangal, Chemical reduction of graphene oxide to graphene by sulfur-containing compounds, J. Phys. Chem. C. 114 (2010) 19885–19890.

[72] J.H. Kang, T. Kim, J. Choi, J. Park, Y.S. Kim, M.S. Chang, H. Jung, K.T. Park, S.J. Yang, C.R. Park, Hidden Second Oxidation Step of Hummers Method, Chem. Mater. 28 (2016) 756–764.

[73] S. Eigler, C. Dotzer, A. Hirsch, M. Enzelberger, P. Müller, Formation and decomposition of CO_2 intercalated graphene oxide, Chem. Mater. 24 (2012) 1276–1282.

[74] Z. Sofer, O. Jankovský, P. Šimek, D. Sedmidubský, J. Šturala, J. Kosina, R. Mikšová, A. Macková, M. Mikulics, M. Pumera, Insight into the mechanism of the thermal reduction of graphite oxide: Deuterium-labeled graphite oxide is the key, ACS Nano. 9 (2015) 5478–5485.

[75] A. Bagri, C. Mattevi, M. Acik, Y.J. Chabal, M. Chhowalla, V.B. Shenoy, Structural evolution during the reduction of chemically derived graphene oxide, Nat. Chem. 2 (2010) 581–587.

[76] I. Dékány, T. Szabó, O. Berkesi, P. Forgó, K. Josepovits, Y. Sanakis, D. Petridis, Evolution of Surface Functional Groups in a Series of Progressively Oxidized Graphite Oxides Evolution of Surface Functional Groups in a Series of Progressively Oxidized Graphite Oxides, Chem. Mater. 18 (2006) 2740–2749.

[77] A. Nikolakopoulou, D. Tasis, L. Sygellou, V. Dracopoulos, C. Galiotis, P. Lianos, Study of the thermal reduction of graphene oxide and of its application as electrocatalyst in quasi-solid state dye-sensitized solarcells in combination with PEDOT, Electrochim. Acta. 111 (2013) 698–706.

[78] F. Wu, J. Li, Y. Tian, Y. Su, J. Wang, W. Yang, N. Li, S. Chen, L. Bao, 3D coral-like nitrogen-sulfur co-doped carbon-sulfur composite for high

performance lithium-sulfur batteries, Sci. Rep. 5 (2015) 13340.

[79] H. Aguilar-Bolados, D. Vargas-Astudillo, M. Yazdani-Pedram, G. Acosta-Villavicencio, P. Fuentealba, A. Contreras-Cid, R. Verdejo, M.A. López-Manchado, Facile and Scalable One-Step Method for Amination of Graphene Using Leuckart Reaction, Chem. Mater. 29 (2017) 6698–6705.

[80] D. Yang, A. Velamakanni, G. Bozoklu, S. Park, M. Stoller, R.D. Piner, S. Stankovich, I. Jung, D.A. Field, C.A. Ventrice, R.S. Ruoff, Chemical analysis of graphene oxide films after heat and chemical treatments by X-ray photoelectron and Micro-Raman spectroscopy, Carbon. 47 (2009) 145–152.

[81] H. Li, Z. Song, X. Zhang, Y. Huang, S. Li, Y. Mao, H.J. Ploehn, Y. Bao, M. Yu, Ultrathin, molecular-sieving graphene oxide membranes for selective hydrogen separation, Science. 342 (2013) 95–98.

[82] N. Xiao, X. Dong, L. Song, D. Liu, Y. Tay, S. Wu, L.J. Li, Y. Zhao, T. Yu, H. Zhang, W. Huang, H.H. Hng, P.M. Ajayan, Q. Yan, Enhanced thermopower of graphene films with oxygen plasma treatment, ACS Nano. 5 (2011) 2749–2755.

[83] K.N. Kudin, B. Ozbas, H.C. Schniepp, R.K. Prud'homme, I.A. Aksay, R. Car, Raman Spectra of Graphite Oxide and Functionalized Graphene Sheets, Nano Lett. 8 (2008) 36–41.

[84] M.M. Lucchese, F. Stavale, E.H.M. Ferreira, C. Vilani, M.V.O. Moutinho, R.B. Capaz, C.A. Achete, A. Jorio, Quantifying ion-induced defects and Raman relaxation length in graphene, Carbon. 48 (2010) 1592–1597.

[85] G. Wang, X. Sun, C. Liu, J. Lian, Tailoring oxidation degrees of graphene oxide by simple chemical reactions, Appl. Phys. Lett. 99 (2011) 053114.

[86] W. Gao, L.B. Alemany, L. Ci, P.M. Ajayan, New insights into the structure and reduction of graphite oxide, Nat. Chem. 1 (2009) 403–408.

[87] S. Hun, Thermal Reduction of Graphene Oxide, in: Phys. Appl. Graphene - Exp., InTech, 2011: pp. 73–90.

[88] A. Bagri, C. Mattevi, M. Acik, Y.J. Chabal, M. Chhowalla, V.B. Shenoy, Structural evolution during the reduction of chemically derived graphene oxide, Nat. Chem. 2 (2010) 581–587.

[89] A. Lerf, H. He, M. Forster, J. Klinowski, Structure of Graphite Oxide Revisited ‖, J. Phys. Chem. B. 102 (1998) 4477–4482.

[90] Q. Yang, Y. Su, C. Chi, C.T. Cherian, K. Huang, V.G. Kravets, F.C. Wang, J.C. Zhang, A. Pratt, A.N. Grigorenko, F. Guinea, A.K. Geim, R.R. Nair, Ultrathin graphene-based membrane with precise molecular sieving and ultrafast solvent permeation, Nat. Mater. 16 (2017) 1198–1202.

[91] A. Akbari, P. Sheath, S.T. Martin, D.B. Shinde, M. Shaibani, P.C. Banerjee, R. Tkacz, D. Bhattacharyya, M. Majumder, Large-area graphene-based nanofiltration membranes by shear alignment of discotic nematic liquid crystals of graphene oxide, Nat. Commun. 7 (2016) 10891.

[92] A. Klechikov, J. Yu, D. Thomas, T. Sharifi, A. V. Talyzin, Structure of graphene oxide membranes in solvents and solutions, Nanoscale. 7 (2015) 15374–15384.

[93] K.S. Andrikopoulos, G. Bounos, D. Tasis, L. Sygellou, V. Drakopoulos, G.A. Voyiatzis, The Effect of Thermal Reduction on the Water Vapor Permeation in Graphene Oxide Membranes, Adv. Mater. Interfaces. 1 (2014) 1400250.

[94] T. Van Gestel, J. Barthel, New types of graphene-based membranes with molecular sieve properties for He, H_2 and H_2O, J. Memb. Sci. 554 (2018) 378–384.

[95] V. Barranco, M.A. Lillo-Rodenas, A. Linares-Solano, A. Oya, F. Pico, J. Ibañez, F. Agullo-Rueda, J.M. Amarilla, J.M. Rojo, Amorphous Carbon Nanofibers and Their Activated Carbon Nanofibers as Supercapacitor Electrodes, J. Phys. Chem. C. 114 (2010) 10302–10307.

[96] E. Raymundo-Piñero, P. Azaïs, T. Cacciaguerra, D. Cazorla-Amorós, A. Linares-Solano, F. Béguin, KOH and NaOH activation mechanisms of multiwalled carbon nanotubes with different structural organisation, Carbon. 43 (2005) 786–795.

[97] M.A. Lillo-Ródenas, D. Cazorla-Amorós, A. Linares-Solano, Understanding chemical reactions between carbons and NaOH and KOH: An insight into the chemical activation mechanism, Carbon. 41 (2003) 267–275.

[98] M.A. Lillo-Ródenas, D. Lozano-Castelló, D. Cazorla-Amorós, A. Linares-Solano, Preparation of activated carbons from Spanish anthracite - II. Activation by NaOH, Carbon. 39 (2001) 751–759.

[99] S. Kim, K. Choi, Y. Shim, S. Lee, S. Park, The Effect of KOH Treatment on the Chemical Structure and Electrocatalytic Activity of Reduced Graphene Oxide Materials, Chem. - A Eur. J. 22 (2016) 11435–11440.

[100] M.A. Lillo-Ródenas, J. Juan-Juan, D. Cazorla-Amorós, A. Linares-Solano, About reactions occurring during chemical activation with hydroxides, Carbon. 42 (2004) 1365–1369.

[101] B. Zdravkov, J.J. Čermák, J. Janků, V. Kučerová, M. Šefara, Pore classification in the characterization of porous materials, Chem. List. 102 (2008) 434–438.

[102] J. Rouquerol, D. Avnir, C.W. Fairbridge, D.H. Everett, J.M. Haynes, N. Pernicone, J.D.F. Ramsay, K.S.W. Sing, K.K. Unger, Recommendations for the characterization of porous solids (Technical Report), Pure Appl. Chem. 66 (1994) 1739–1758.

[103] K.S.W. Sing, Reporting physisorption data for gas/solid systems with special reference to the determination of surface area and porosity (Recommendations 1984), Pure Appl. Chem. 57 (1985) 603–619.

[104] H. Schultz, G. Bauer, E. Schachl, F. Hagedorn, P. Schmittinger, Potassium Compounds, in: Ullmann's Encycl. Ind. Chem., Wiley-VCH Verlag GmbH & Co. KGaA, Weinheim, Germany, 2012: pp. 639–704.

[105] C. Chen, T. Tran, R. Olivares, S. Wright, S. Sun, Coupled Experimental Study and Thermodynamic Modeling of Melting Point and Thermal Stability of Li_2CO_3 - Na_2CO_3 - K_2CO_3 Based Salts, J. Sol. Energy Eng. 136 (2014) 031017.

[106] D. Li, M.B. Müller, S. Gilje, R.B. Kaner, G.G. Wallace, Processable aqueous dispersions of graphene nanosheets, Nat. Nanotechnol. 3 (2008) 101–105.

[107] Z. Tan, G. Chen, Y. Zhu, Carbon-Based Supercapacitors Produced by the Activation of Graphene, Nanocarbons Adv. Energy Storage. 1 (2015) 211–225.

[108] K. Huang, G. Liu, J. Shen, Z. Chu, H. Zhou, X. Gu, W. Jin, N. Xu, High-Efficiency Water-Transport Channels using the Synergistic Effect of a Hydrophilic Polymer and Graphene Oxide Laminates, Adv. Funct. Mater. 25 (2015) 5809–5815.

[109] Y. Wang, S. Chen, L. Qiu, K. Wang, H. Wang, G.P. Simon, D. Li, Graphene-directed supramolecular assembly of multifunctional polymer hydrogel membranes, Adv. Funct. Mater. 25 (2015) 126–133.

[110] V. Boffa, H. Etmimi, P.E. Mallon, H.Z. Tao, G. Magnacca, Y.Z. Yue, Carbon-based building blocks for alcohol dehydration membranes with disorder-

enhanced water permeability, Carbon. 118 (2017) 458–466.

[111] M.A.C. Stuart, W.T.S. Huck, J. Genzer, M. Müller, C. Ober, M. Stamm, G.B. Sukhorukov, I. Szleifer, V. V. Tsukruk, M. Urban, F. Winnik, S. Zauscher, I. Luzinov, S. Minko, Emerging applications of stimuli-responsive polymer materials, Nat. Mater. 9 (2010) 101–113.

[112] K. König, V. Boffa, B. Buchbjerg, A. Farsi, M.L. Christensen, G. Magnacca, Y. Yue, One-step deposition of ultrafiltration SiC membranes on macroporous SiC supports, J. Memb. Sci. 472 (2014) 232–240.

[113] T. Kaneko, D. Nemoto, A. Horiguchi, N. Miyakawa, FTIR analysis of a-SiC:H films grown by plasma enhanced CVD, J. Cryst. Growth. 275 (2005) e1097–e1101.

[114] J.P. Conde, V. Chu, M.F. Da Silva, A. Kling, Z. Dai, J.C. Soares, S. Arekat, A. Fedorov, M.N. Berberan-Santos, F. Giorgis, C.F. Pirri, Optoelectronic and structural properties of amorphous silicon-carbon alloys deposited by low-power electron-cyclotron resonance plasma-enhanced chemical-vapor deposition, J. Appl. Phys. 85 (1999) 3327–3338.

[115] D.S. Kim, Y.H. Lee, Room-temperature deposition of a-SiC:H thin films by ion-assisted plasma-enhanced CVD, Thin Solid Films. 283 (1996) 109–118.

[116] D. Panda, A. Nandi, S.K. Datta, H. Saha, S. Majumdar, Selective detection of carbon monoxide (CO) gas by reduced graphene oxide (rGO) at room temperature, RSC Adv. 6 (2016) 47337–47348.

[117] S. Samanta, S. Singh, R.R. Sahoo, Simultaneous chemical reduction and surface functionalization of graphene oxide for efficient lubrication of steel-steel contact, RSC Adv. 5 (2015) 61888–61899.

[118] A. Kozbial, Z. Li, C. Conaway, R. McGinley, S. Dhingra, V. Vahdat, F. Zhou, B. D'Urso, H. Liu, L. Li, Study on the Surface Energy of Graphene by Contact Angle Measurements, Langmuir. 30 (2014) 8598–8606.

ISSN (online): 2446-1636
ISBN (online): 978-87-7210-392-1

AALBORG UNIVERSITY PRESS